OUKA

The University of Osaka
Institutional Knowledge Archive

Title	The Whole Structure of the 13-Subunit Oxidized Cytochrome c Oxidase from Bovine Heart at 2.8 Å Resolution
Author(s)	Yamashita, Eiki
Citation	大阪大学, 1997, 博士論文
Version Type	VoR
URL	https://doi.org/10.11501/3128865
rights	
Note	

The University of Osaka Institutional Knowledge Archive : OUKA

https://ir.library.osaka-u.ac.jp/

The University of Osaka

The Whole Structure of the 13-Subunit Oxidized Cytochrome *c* Oxidase from Bovine Heart at 2.8 Å Resolution

A Doctoral Thesis

by

Eiki Yamashita

Submitted to the Graduate School

of Science, Osaka University

Japan

February, 1997

The Whole Structure of the 13-Subunit Oxidized Cytochrome *c* Oxidase from Bovine Heart at 2.8 Å Resolution

A Doctoral Thesis

by

Eiki Yamashita

Submitted to the Graduate School

of Science, Osaka University

Japan

February, 1997

Approval

February, 1997

This thesis is approved as to

style and content by

月原冒武

Member-in-chief

中村晃   油后克英

Member   Member

上山憲一

Member

Acknowledgments

The present work has been carried out under the direction of Professor Tomitake Tsukihara of Institute for Protein Research, Osaka University. I would like to thank him for his incessant guidance and encouragement throughout this work. I am deeply indebted to Professor Shinya Yoshikawa, Himeji Institute of Technology, for his invaluable advice and discussion. I am also grateful to Dr. Kyoko Shinzawa-Ito, Himeji Institute of Technology, for her technical advice and helpful suggestion.

I am deeply grateful to Associate Professor Yukio Morimoto, Himeji Institute of Technology, for his incessant encouragement and helpful advice to X-ray crystallography. I am also grateful to Dr. Takao Sato, Tokushima University, for his valuable suggestion. I am deeply indebted to Dr. Hiroshi Aoyama, The Institute of Physical and Chemical Research, and Mr. Takashi Tomizaki, European Molecular Biological Laboratory, for their assistance.

I also wish sincere thanks to Associate Professor Yoshiki Matsuura, Associate Professor Masami Kusunoki

and Dr. Hiroshi Yamaguchi of Institute for Protein Research, Osaka University.

I am deeply grateful to Professor Noriyoshi Sakabe. Dr. Atsushi Nakagawa, Nobuhisa Watanabe and Shinji Ikemizu of Photon Factory, National Laboratory for High Energy Physics for their help in data collection by means of the Weissenberg camera and synchrotron radiation.

I am deeply grateful to Professor Mamoru Sato of Yokohama City University, and Dr. Yasuyuki Kitagawa of Showa University School of Medicine for their useful help and discussion in X-ray structure study.

I express my thanks to all members in Tsukihara's and Yoshikawa's laboratories for kind assistances and encouragement.

Finally, I thank my parents for their incessant understanding and encouragement.

山下栄樹

Eiki Yamashita

February, 1997

Contents

Chapter 1.

Introduction

Cytochrome c oxidase (EC 1.9.3.1), a multicomponent membrane protein, is the terminal oxidase of the mitochondrial respiratory chain in mammals and of the energy-transducing electron transfer chains of certain bacteria. This enzyme catalyzes the transfer of electrons from reduced cytochrome c to molecular oxygen to produce water. In the process, four protons are consumed as shown in the equation:

$$4H^+ + 4e^- + O_2 \rightarrow 2H_2O$$
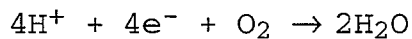
The four protons are taken up from the interior (mitochondrial matrix space in mammals and bacterial cytoplasmic space in bacteria). In addition, using the energy released in the oxidation-reduction reaction, the enzyme pumps four additional protons from the interior to the exterior (mitochondrial intermembrane space and bacterial periplasmic space) (Malmström, 1990; Babcock & Wikström, 1992). The electrochemical proton gradient across energy-transducing membrane produced by these reactions is used to generate ATP. This enzyme is ubiquitous among aerobic organisms from bacteria to mammals. In prokaryotes, cytochrome c

oxidase is a component of the cytoplasmic membrane, in eukaryotes the enzyme is localized to mitochondrial inner membrane. They all contain four prosthetic groups, two heme a's and two copper sites. However, the number of subunits is diverse; ranging from three in *Rhodobacter sphaeroides* enzyme to thirteen in mammalian one. Because of physiological importance and the intriguing reaction catalyzed, the enzyme has been studied as one of the most important subjects in bioenergetics since the discovery of this enzyme by Warburg (1929).

Bovine heart cytochrome *c* oxidase is an integral protein incorporated in the mitochondrial inner membrane, which reduces molecular oxygen to water, coupled with pumping protons from the matrix side of the mitochondrial inner membrane toward the cytosolic side (intermembrane space), as shown in Figure 1.1. This enzyme contains two iron sites (Fe_a and Fe_{a3}) and two copper sites (Cu_A and Cu_B), which are redox centers, in addition to zinc and magnesium sites (Malmström, 1990; Capaldi, 1990). The protein moiety with molecular weight of 200K is composed of thirteen distinct polypeptide subunits (Kadenbach *et al.*, 1983)
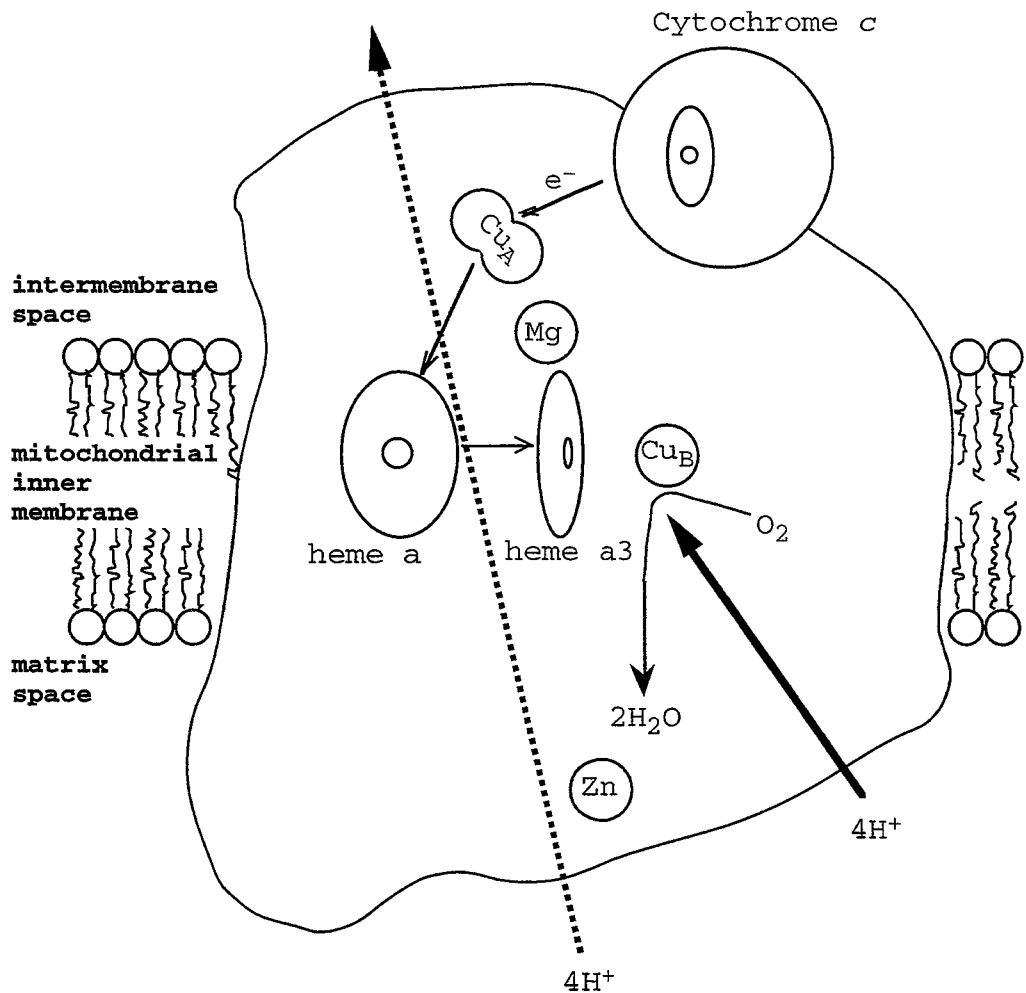
Figure 1.1. Schematic drawing of bovine heart cyotchrome *c* oxidase.

ranging in molecular weight from 57,000 down to 5,000 daltons.

Cytochrome *c* oxidase exhibits a bright green color due to the heme iron. The color is sensitive to the redox and ligand-binding states of the active center. Resonance Raman and infrared spectroscopic studies of enzymatic turnover have been reported by several authors (Malmström, 1990; Babcock & Wikström, 1992; Einersdottir et al., 1993). Electron spin resonance studies have also been made on the paramagnetic iron and copper ions (Malmström, 1990; Babcock & Wikström, 1992), and infrared spectroscopy has been used to study various respiratory inhibitors as probes of the O_2 binding site (Caughey et al., 1993). In addition, the varied roles of large and complex protein moiety have been widely investigated (Capaldi, 1990; Kadenbach, 1981; 1983).

The three-dimensional structure of monomer of bovine heart cytochrome *c* oxidase at low resolution was obtained by electron microscopy of two-dimensional crystals (Fuller et al., 1979). The monomer resembles the shape of lop-sided y, as shown in Figure 1.2, with a height of approximately 110 Å. The domains which form the arms of the y (M1 and M2) are roughly 50 Å in
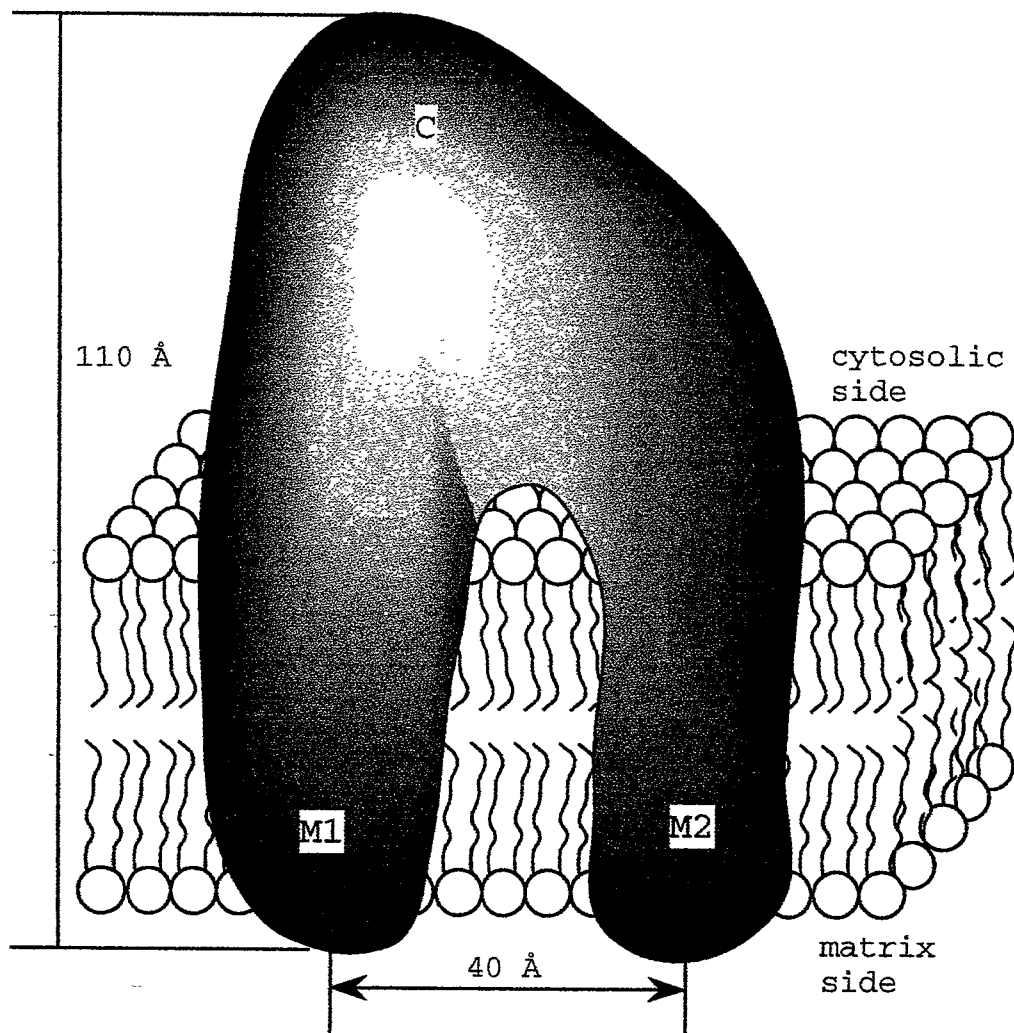
4

Figure 1.2. Structure model for cytochrome *c* oxidase showing y-shaped monomer by electron microscope.
M1 and M2 are the matrix side domains and C is the cytosolic side domain.

length and have a center to center separation of 40 Å. These domains protrude slightly on mitochondrial matrix side of the membrane. The cytoplasmic side of the molecule is composed of a single large domain (C) of roughly 55 Å.

The enzyme from bovine heart is a hybrid-protein since it is composed of subunits coded for by both mitochondrial DNA and nuclear DNA. The amino acid sequences of the three larger subunits which are encoded by mitochondrial DNA were deduced from the complete mitochondrial DNA sequence (Anderson *et al.*, 1982). The complete amino acid sequences of eight of the nuclear coded subunits: **IV**, **Vb**, **VIa**, **VIb**, **VIc**, **VIIa**, **VIIc**, and **VIII**, were determined directly by Buse and co-workers (Buse *et al.*, 1978; Satcher *et al.*, 1979; Steffens *et al.*, 1979; Biewald *et al.*, 1982; Meinecke *et al.*, 1984; 1985; 1986; Erdweg *et al.*, 1985). The amino acid sequence of subunit **Va** was determined by Tanaka *et al.* (1979) and that of subunit **VIIb** by Yanamura *et al.* (1988). The enzyme of monomer consists of 1803 amino acids summing up to a total molecular weight of 204,005. The molecular weight and number of amino acid residue of each of the subunits are listed in Table 1.1.

Table 1.1. Number of residues and the molecular weight of each subunit of bovine heart cytochrome *c* oxidase.

Subunit number	Number of residues	Molecular weight
I	514	57017.11
II	227	26004.63
III	261	29902.15
IV	147	17134.35
Va	109	12418.32
Vb	98	10652.24
VIa	84	9417.97
VIb	85	10007.32
VIc	73	8460.92
VIIa	56	6262.40
VIIb	56	6339.35
VIIc	47	5423.45
VIII	46	4943.70

Hydropathy plots of the subunits synthesized in the mitochondria predict that subunit **I** has twelve possible transmembrane helices, subunit **II** has two, and subunit **III** has seven (Raitio *et al.*, 1987; Muller *et al.*, 1988; Capaldi, 1990). Seven of ten nuclear-coded subunits have a tripartite structure with a hydrophilic NH_2-terminus, a hydrophobic central domain exhibiting a helical structure, and a hydrophilic COOH-terminus. These subunits are labeled by lipophilic reagents designed to react with protein from within the bilayer. Thus it was predicted that there were as many as twenty-eight possible transmembrane helices in the enzyme complex. Subunits **Va Vb** and **VIb** do not have hydrophobic domains long enough to span the transmembrane region and are not labeled by lipophilic reagents. Therefore, they were thought to be extramembrane subunits. The orientations of the nuclear coded subunits had been explored by chemical labeling and protease digestion experiments. Subunits **IV**, **VIc**, and **VIIb** were oriented with their NH_2-termini on the matrix side, and subunit **VIII** with its COOH-terminus on the matrix side. Subunit **VIb** was localized to the cytosolic side (Capaldi, 1990).

The metal composition of cytochrome *c* oxidase has been quite controversial. It was generally agreed that two hemes and at least two copper ions are bound to the enzyme monomer (Malatesta, 1995). Einersdottir *et al.* (1985) found five copper atoms per four hemes and one zinc atom and one magnesium atom per enzyme monomer, using inductively coupled plasma atomic emission spectroscopy. Steffens *et al.* (1987), using the same technique, suggested that there were three copper atoms and two hemes in monomer. Spectroscopic studies and mutagenesis experiments indicated the location and the ligation states of the metal centers in the enzyme as follows. The Cu_A site is ligated by two histidines and two cysteines in subunit **II**. Heme a, heme a_3 and Cu_B are all located in subunit **I** and presumably buried inside the protein between the lipid bilayers. Heme a is ligated by two histidines, heme a_3 by one histidine, and Cu_B by three histidines. Heme a_3 and Cu_B were also suggested to be bridged by a shared ligand, which could be a sulfur containing residue, a μ-peroxy group, or a chloride ion (Capaldi, 1990).

In spite of these extensive and successful efforts, the absence of the three-dimensional structure at atomic resolution has set limits on our

9

understanding of the reaction mechanism of this enzyme. X-ray crystallography is the most powerful technique for determination of the whole three-dimensional structure of a biological macro molecular assembly at atomic resolution. Thus, we undertook the crystal structure analysis of bovine heart cytochrome *c* oxidase to understand the reaction mechanism of this enzyme.

Crystals of cytochrome *c* oxidase isolated from bovine heart muscle have been obtained and the three-dimensional structure was solved at 2.8 Å resolution. Structures of the metal sites and the electron transfer path from initial model have been reported by Aoyama (1996). In chapter 2, the crystal structure refinement of cytochrome *c* oxidase at 2.8 Å resolution is described. In chapter 3, the refined structure of bovine heart cytochrome *c* oxidase is given and discussed. In chapter 4, the possible proton transfer pathways through the structure which is the essential function of this enzyme are discussed in detail. The other possible channels, the O_2 channel and the H_2O channel, found in the three-dimensional structure are described.
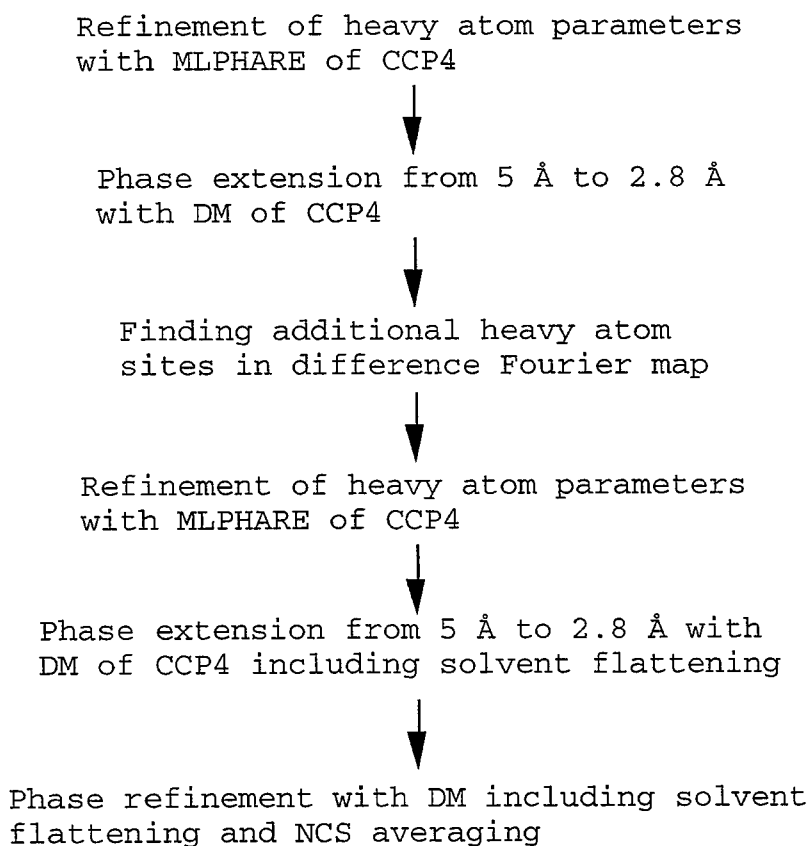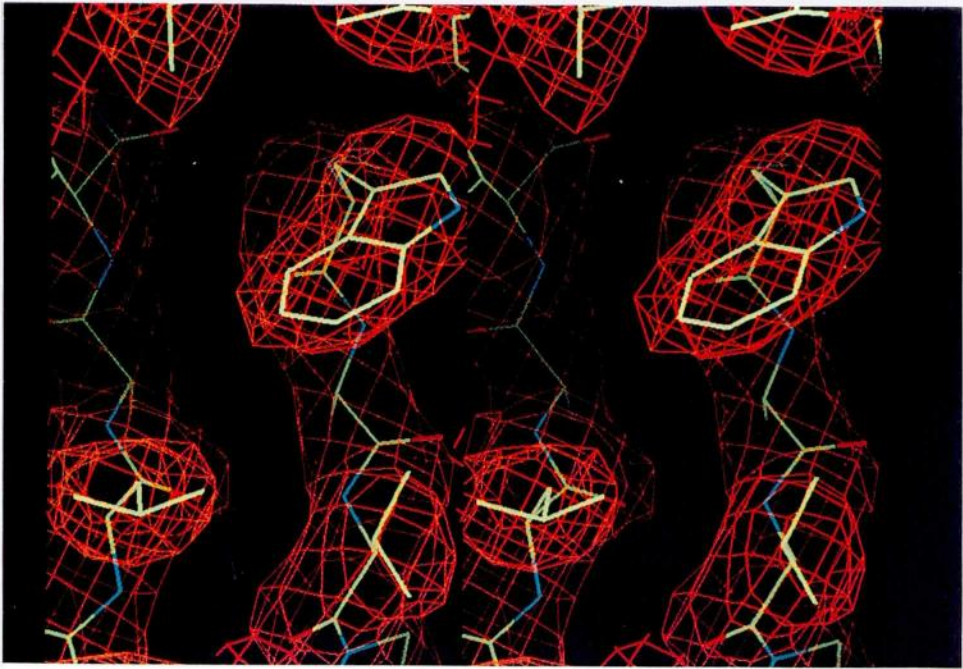
Chapter 2.

Structure refinement of bovine cytochrome *c* oxidase at 2.8 Å resolution

2.1. Model building

The initial electron density map was calculated by the multiple isomorphous replacement (MIR) method (Blow, 1959) using three derivatives: two $IrCl_6^{2-}$ and a CH_3HgCl derivatives. Their heavy atom parameters were refined with the program MLPHARE (Otwinowski, 1991) of the CCP4 program package. The heavy atom refinement and MIR phase determination are summarized in Table 2.1. Further improvement in the phases was performed by the density modification program DM (Cowtan, 1994) of CCP4. The resultant map (MIR-DM map) then used to build the atomic model of cytochrome *c* oxidase at 2.8 Å resolution. An atomic model was built using the X-Fit in the program package QUANTA (CTC Laboratory Systems Co., Ltd.) and the program TURBO FRODO on IRIS workstations. The MIR-DM map was so clear that the molecular model was unambiguous as shown in Figures 2.1a, b and c. The clear electron density distributions of the MIR-DM map are depicted together with polypeptide models in these figures for three typical

Table 2.1. Procedure of phase determination.

Refinement of heavy atom parameters
with MLPHARE of CCP4

↓

Phase extension from 5 Å to 2.8 Å
with DM of CCP4

↓

Finding additional heavy atom
sites in difference Fourier map

↓

Refinement of heavy atom parameters
with MLPHARE of CCP4

↓

Phase extension from 5 Å to 2.8 Å with
DM of CCP4 including solvent flattening

↓

Phase refinement with DM including solvent
flattening and NCS averaging
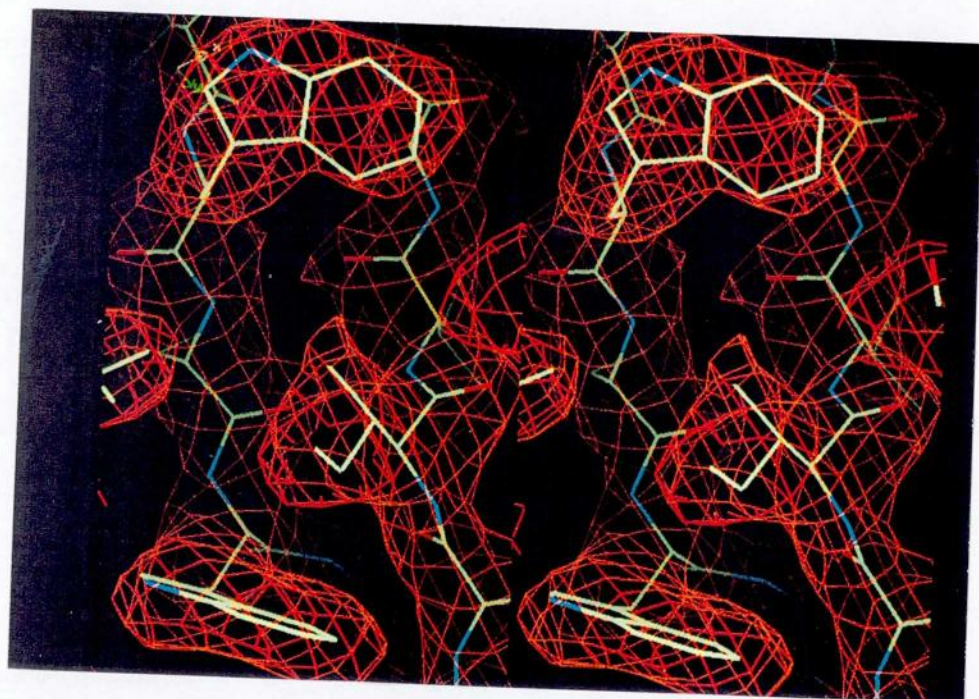
---

a) Cytosolic side of subunit II.

Figure 2.1. Fitting of the atomic model to the DM-MIR map.
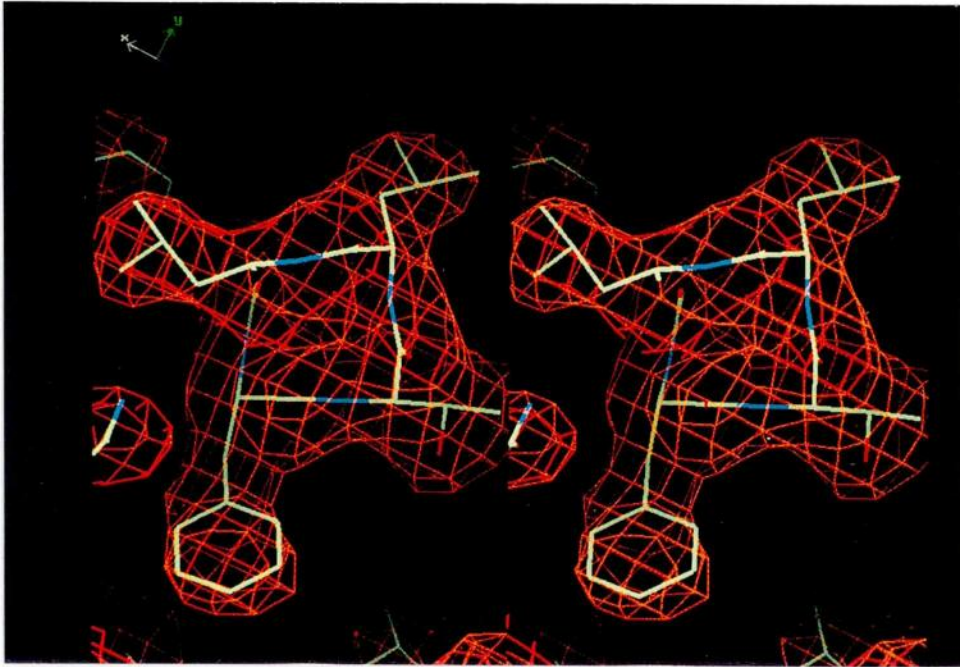
b) Transmembrane region of subunit III.

c) Matrix side of subunit Vb.

regions of the intermembrane side, the transmembrane region and the matrix side. Out of 1803 amino acid residues of thirteen polypeptide subunits in the monomer, 1771 residues with side chains were clearly located in the MIR-DM map and only a few residues were poorly defined in the MIR-DM map. It took only four weeks for us to build the structure of the 1771 residues of the monomer. Almost 100 residues were built up per day. This is one of the quick model building so far as we know. Three phosphatidyl ethanolamines and one phosphatidyl glycerols in the monomer unit were successfully located in the MIR-DM map. The other monomer was generated using non-crystallographic symmetry to construct the dimer structure. The initial model fitted in the MIR-DM map had a total of 28,976 atoms with a crystallographic R-factor of 0.365 in the resolution range 10.0–2.8 Å.

2.2. Crystallographic refinement

The initial model was refined using molecular dynamics refinement (simulated annealing) or positional refinement and temperature factor refinement as implemented in the program X-PLOR (Brünger, 1988). During the course of the refinement, the model was

revised manually in the MIR-DM map. The summary of the structure refinement is shown in Figure 2.2. The parameters used in the X-PLOR refinement for the protein were exchanged for those of Brooks (1983) to those of Engh and Huber (1991) after the convergency of the second round of positional and temperature factor refinement. All refinement processes with X-PLOR were performed with non-crystallographic symmetry restrains. Some amino acid residues which were ambiguous in the MIR-DM map were built successfully in 2Fo-Fc map composed with Fourier coefficients of (2Fo-Fc)exp(iαc), where αc are the calculated phase angles from the partially refined model. Amino acid residues and other phospholipids, cholic acid, and decyl maltoside moieties not included in the initial model of 28,976 non-hydrogen atoms were found out in the difference Fourier map (Fo-Fc map) composed with coefficients of (Fo-Fc)exp(iαc) and the revised structures were also constructed in the MIR-DM map. At the final stage of the refinement, the coordination geometry of metals with the ligand atoms were reasonably adjusted in the Fo-Fc map. Although water molecules have been identified in the MIR-DM map, they were not included in the present refinement.

17
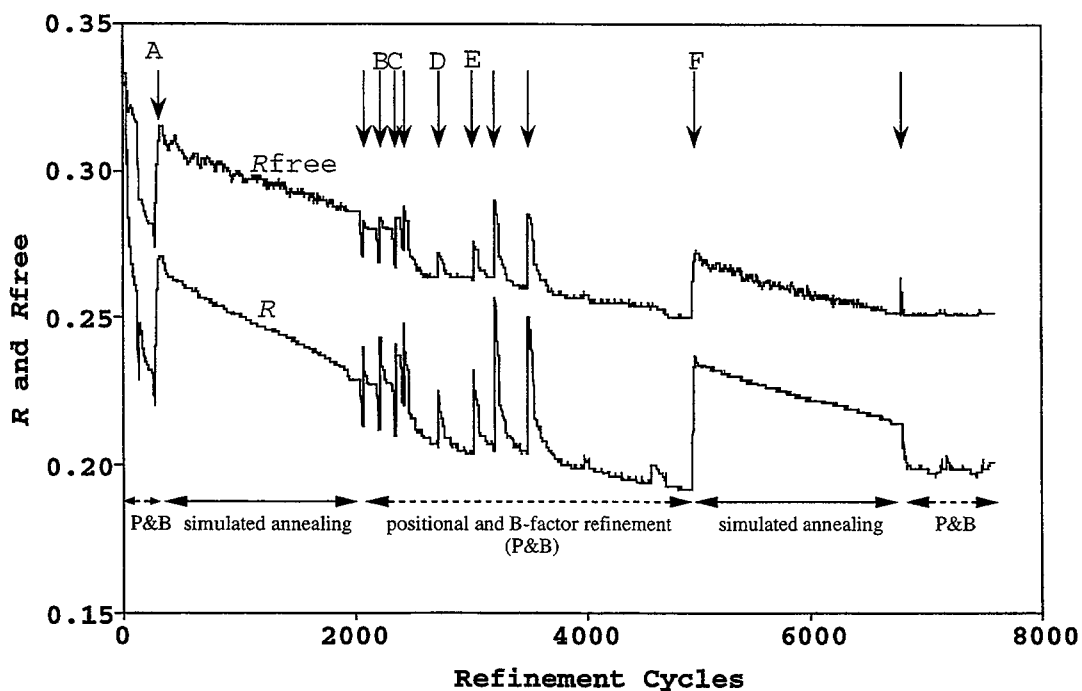
Figure 2.2. A refinement survey of X-PLOR refinement at 2.8 Å resolution.
Manual revisions were done at the stages denoted with an arrow. At the A stage before simulated annealing, five amino acid residues were constructed. At the B stage, two phospholipids were found out. In addition, four residues were built at the C stage. Two phospholipids and two colic acids were found out in the Fo-Fc map and added to the model. The parameters for the protein changed from those of Brooks to those of Engh and Huber at the F stage.

The current refined model consists of a total of 29,808 non-hydrogen atoms, including 3,560 amino acid residues, two hemes a, two hemes a3, six coppers, two zincs, two magnesiums, ten phosphatidyl ethanolamines, six phosphatidyl glycerols, eight cholic acids, and two decyl maltosides. This model gives a crystallographic R factor of 0.199 for 151,622 of observed reflections at 2.8 Å resolution and free R factor (Brünger, 1992) that is calculated from a test set of 5 % of the reflections not used in the refinement, of 0.252. The Ramachandran plot (Ramakrishman, 1965) for 3560 residues are given in Figure 2.3. Out of 3050 non-glycine residues, only 8 residues (0.3%) all of which are in the terminal regions are in the disallowed regions. Reasonable main chain conformations are achieved over the rest of the molecules. The root mean square deviations from standard ideal values are 0.012 Å for bond lengths and 1.6° for bond angles. Averaged r.m.s.d. positional error was estimated to be 0.35 Å from Luzzati plots (Luzzati, 1952), as shown in Figure 2.4.

Figure 2.3. Ramachandran plot for refined model of cytochrome c oxidase.
Triangles represent glycine residues and squares represent non-glycine residues.
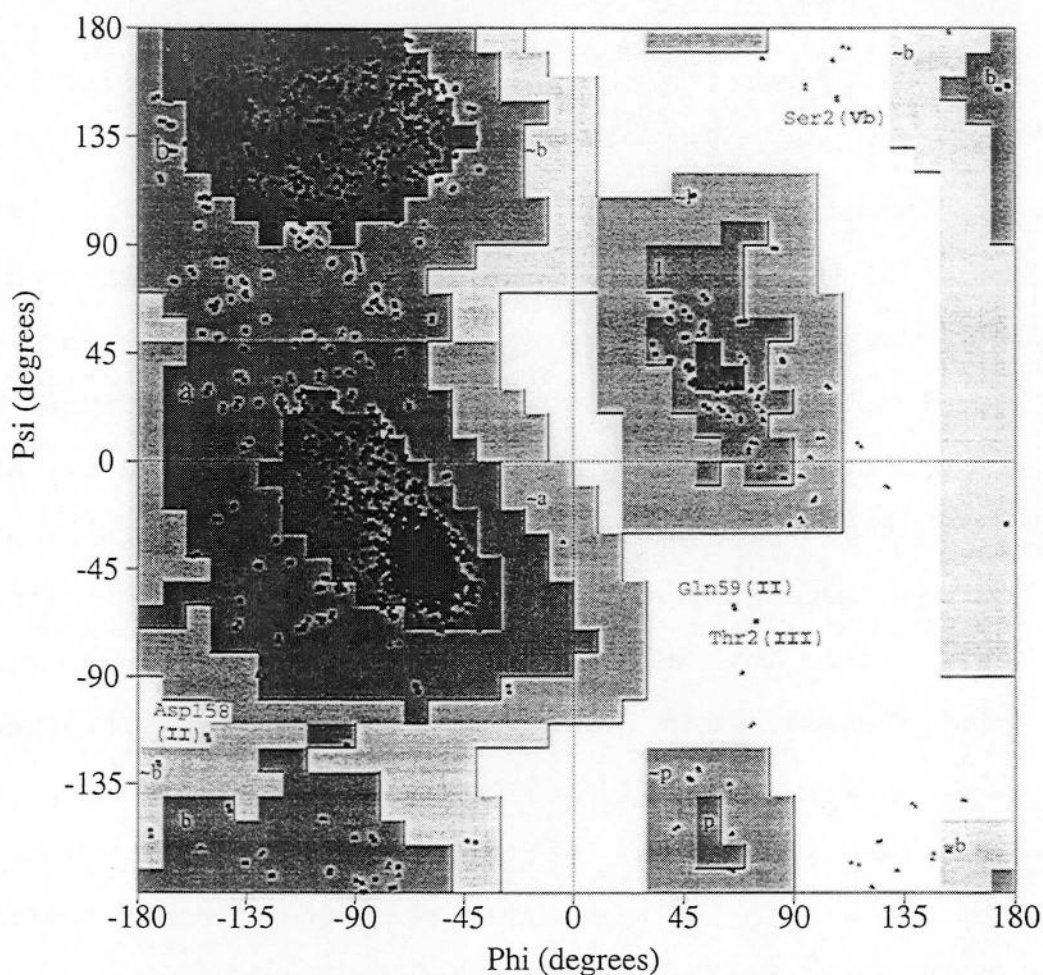
Plot statistics

Residues in most favoured regions [A,B,L]	2729	89.2%
Residues in additional allowed regions [a,b,l,p]	299	9.8%
Residues in generously allowed regions [~a,~b,~l,~p]	22	0.7%
Residues in disallowed regions	8	0.3%
	----	------
Number of non-glycine and non-proline residues	3058	100.0%
Number of end-residues (excl. Gly and Pro)	50	
Number of glycine residues (shown as triangles)	256	
Number of proline residues	196	

Total number of residues	3560	

Based on an analysis of 118 structures of resolution of at least 2.0 Angstroms
and R-factor no greater than 20%, a good quality model would be expected
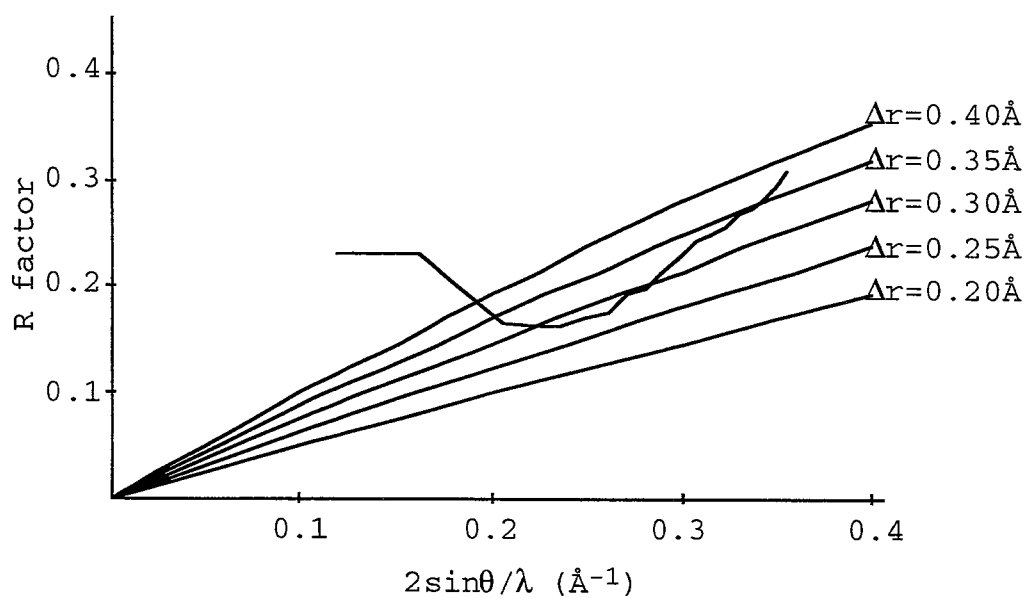to have over 90% in the most favoured regions.

Figure 2.4. The distribuition of R-factors as a function of $2\sin\theta/\lambda$.

21

2.3. Discussion of the structure analysis

Looking back the whole process of the crystal structure analysis at 2.8 Å resolution, we think that the successful interpretation of each difference Patterson map at 5 Å resolution was the most critical step to solve the phase problem. When the asymmetric unit with a total molecular weight of 400K is taken into account, $IrCl_6^{2-}$ and CH_3HgCl seem to be so small that the interpretation of their difference Patterson maps could be expected to have been very difficult. Previously, the accuracy of the observed intensity of the weak reflections for the native had been thought not to be important, because their contributions to the electron density are negligible in comparison with strong reflections. Thus special care was not taken for intensity data collections of weak reflections in earlier data collections. However, since the heavy atom contribution to each reflection is independent of magnitude of the native structure amplitude, accurate observation of intensities of the reflections with weak native structure amplitudes can produce a clear difference Patterson map. This is the most likely reason why the heavy atom derivatives of the present crystal form were successfully interpreted.

Heavy atom positions of each derivative are listed in Table 2.2. All the heavy atoms introduced into the derivatives are on the molecular surface of the intermembrane space and the matrix side which was expected. As $IrCl_6^{2-}$ is not commonly used to prepare a heavy atom derivative, its binding sites were not known well. The $IrCl_6^{2-}$ groups are located closely at carboxyl groups, $S\delta$ atoms of Met residues, $S\gamma$ atoms of Cys residues, $N\varepsilon2$ atoms of His residues and carbonyl atoms of peptide bonds. One of the Cl ion coordinating to the Ir ion must be replaced by one of these atoms with lone pair electrons. As these groups exist in any protein, this reagent will be useful for other protein crystals, too.

As previously described, the MIR-DM map was so clear that the initial model constructed in the map resulted in the low crystallographic R-factor of 0.365. The implication is that solvent flattening and non-crystallographic averaging are very powerful tools when applied to the phase refinement of the present crystal. Most of the membrane protein complexes solved contain solvent molecules in similar amounts to the cytochrome *c* oxidase (73 % of the asymmetric unit by volume), and their crystals often more than two molecules in the

asymmetric unit. Therefore, solvent flattening and non-crystallographic averaging can be applied to the crystal structure analysis of membrane protein crystals in general.

In the Luzzati plots, the R-factor increase at high resolution. This is because of limited data accuracy at the resolution range higher than 3.0 Å.

Table 2.2 Refined heavy-atom site

	X	Y	Z	Subunit	Surrounding atom		Distance
IrCl$_6$(I)	0.275	0.447	0.783	A-VIIc	Glu16	Oε1	2.81Å
						Oε2	2.05Å

	X	Y	Z	Subunit	Surrounding atom		Distance
IrCl$_6$(II)	0.275	0.447	0.783	A-VIIc	Glu16	Oε1	2.81Å
						Oε2	2.05Å
	0.204	0.394	0.780	A-I	Met1	Sδ	1.69Å
				A-VIIc	His2	O	3.91Å
	0.242	0.074	0.743	B-I	Met1	Sδ	2.25Å
				B-VIIc	His2	O	3.34Å
	0.018	0.449	0.430	A-III	Cys115	Sγ	3.67Å
	0.021	0.020	0.071	B-III	Cys115	Sγ	3.27Å
	0.001	0.426	0.714	A-III	Glu236	Oε1	1.69Å
				A-III	His148	Nε2	2.35Å
	0.032	0.040	0.785	B-III	Glu236	Oε1	1.71Å
				B-III	His148	Nε2	2.87Å
	0.470	0.068	0.281	A-III	Met152	Sδ	1.98Å
	−0.001	0.036	0.779	B-III	Met152	Sδ	2.24Å

	X	Y	Z	Subunit	Surrounding atom		Distance
CH$_3$HgCl	0.393	0.429	0.308	A-Vb	Cys60	Sγ	2.41Å
				A-Vb	Cys85	Sγ	3.26Å
				A-I	Lys514	Nζ	3.00Å
				A-Vb	Tyr89	Oη	3.76Å
				A-Vb	Thr87	Oγ1	3.23Å
				Zn			3.02Å
	0.353	0.099	0.205	B-Vb	Cys60	Sγ	2.13Å
				B-Vb	Cys85	Sγ	3.66Å
				B-I	Lys514	Nζ	2.71Å
				B-Vb	Tyr89	Oη	3.10Å
				B-Vb	Thr87	Oγ1	3.29Å
				Zn			3.21Å
	0.283	0.488	0.277	A-I	Cys498	Sγ	2.30Å
	0.245	0.041	0.250	B-I	Cys498	Sγ	3.10Å
	0.181	0.363	0.671	A-VIIa	Met36	Sδ	3.98Å
						O	3.79
				A-III	Leu22	Cδ2	2.65Å
				A-VIIa	Leu40	Cδ2	2.92Å
	0.206	0.107	0.853	B-VIIa	Met36	Sδ	4.15Å
						O	3.66
				B-III	Leu22	Cδ2	2.78Å
				B-VIIa	Leu40	Cδ2	2.83Å
	0.225	0.350	0.538	A-VIIc	Phe55	O	3.53Å
				A-VIIc	Trp52	O	3.14Å
	0.237	0.118	0.990	B-VIIc	Phe55	O	3.15Å
				B-VIIc	Trp52	O	3.01Å

|						
0.166	0.439	0.100	A-VIIb	Cys25	Sγ	2.10Å
0.148	0.092	0.440	B-VIIb	Cys25	Sγ	1.99Å
-0.001	0.427	0.718	A-III	His232	Nε2	3.20Å
			A-III	Glu236	Oε1	2.05Å
			A-III	His148	Nε2	2.86Å
0.031	0.042	0.785	B-III	His232	Nε2	3.33Å
			B-III	Glu236	Oε1	1.88Å
			B-III	His148	Nε2	2.71Å
0.461	0.064	0.315	A-III	His149	Nε2	2.76Å
0.490	0.467	0.187	B-III	His149	Nε2	2.98Å
0.432	0.105	0.429	A-VIa	Cys31	Sγ	1.99Å
0.450	0.425	0.077	B-VIa	Cys31	Sγ	1.49Å
0.243	0.489	0.149	A-I	His413	Nε2	2.38Å
			A-I	Met468	Sδ	3.88Å
			A-I	Met417	Sδ	3.81Å
			A-I	Met390	Sδ	3.59Å
0.219	0.043	0.379	B-I	His413	Nε2	2.38Å
			B-I	Met468	Sδ	3.88Å
			B-I	Met417	Sδ	3.81Å
			B-I	Met390	Sδ	3.59Å
0.367	0.427	0.301	A-Vb	Cys82	Sγ	1.10Å
			A-Vb	Ser84	Oγ	2.41Å
			A-Vb	Cys62	Sγ	2.79Å
			Zn			2.07Å
0.328	0.103	0.215	B-Vb	Cys82	Sγ	0.82Å
			B-Vb	Ser84	Oγ	2.74Å
			B-Vb	Cys62	Sγ	3.07Å
			Zn			2.03Å
0.377	0.406	0.276	A-Vb	Asn66	Oδ1	3.39Å
0.194	0.359	0.577	A-III	Met33	Sδ	2.72Å
			A-VIIa	Cys49	Sγ	3.53Å
0.176	0.444	0.418	A-II	Tyr105	Oη	3.91Å
			A-II	His102	Cδ2	1.85Å

Chapter 3.

Structure of cytochrome *c* oxidase

3.1. Overall protein structure

The asymmetric unit of the unit cell is composed of two monomers, each containing thirteen different polypeptide subunits as shown in Figure 3.1. Two monomers related by a pseudo two-fold axis produced by combination of a crystallographic two-fold screw axis and a pseudo B face center symmetry to form a dimeric structure. The pseudo two-fold axis is perpendicular to the membrane plane. The dimer has an oval column shape of 90 X 150 Å with 130 Å height. Polar amino acid residues occur chiefly at the top and bottom of the molecule (Figure 3.2). The middle portion is abundant in hydrophobic residues and is composed of 56 α helices in the dimer (Figures 3.1a and 3.3) that form the transmembrane part of the molecule.

All the peptides in the transmembrane region (defined as above) except for the ten amino acid residues in the NH_2-terminal of subunit **VIa** and two segments of the inter-helix regions from Gly121 to Tyr129 and from Val287 to Met292 in subunit **I**, are in α-helical conformation. Comparison of our three-

27
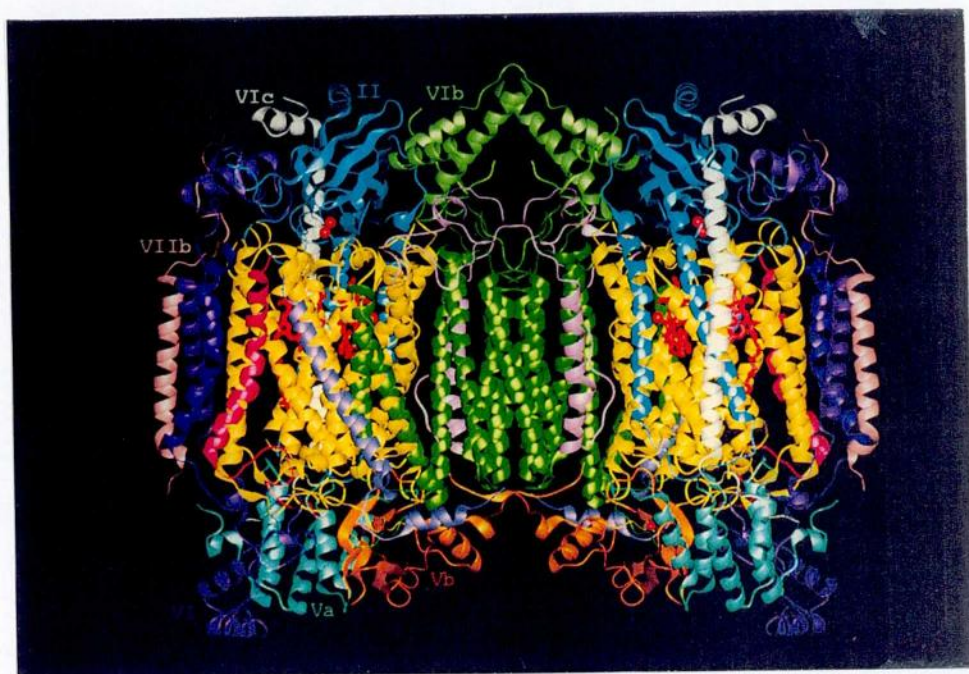
(a) A view to the transmembrane surface.

**Figure 3.1. The ribbon drawings of the dimer of bovine
heart cytochrome _c_ oxidase.**
Each monomer consists of 13 different subunits. Figures
contain hemes a and a3 and three Cu atoms (red). Each
subunit has a different color with the subunit name in
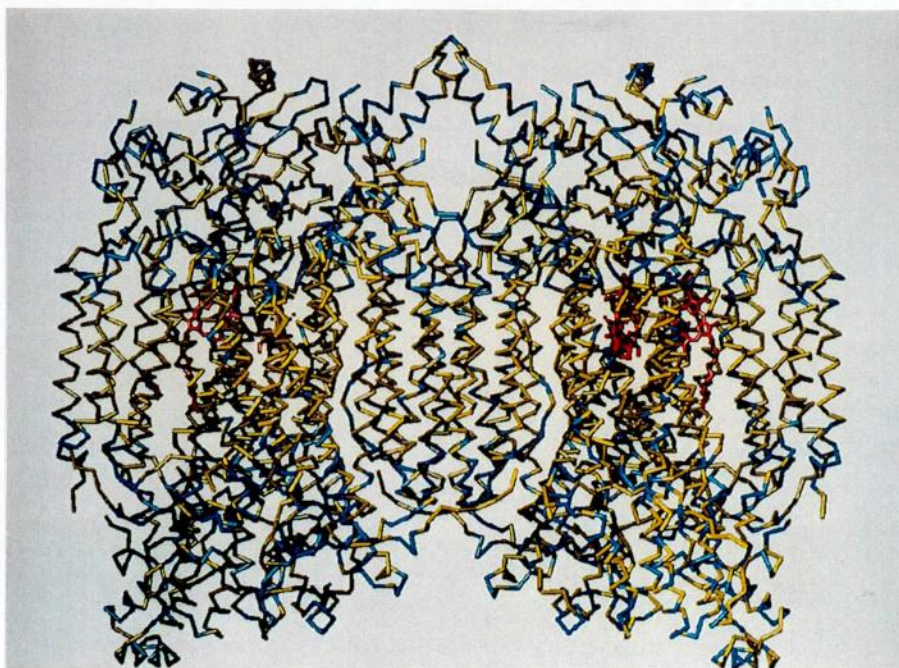the color of the subunit.
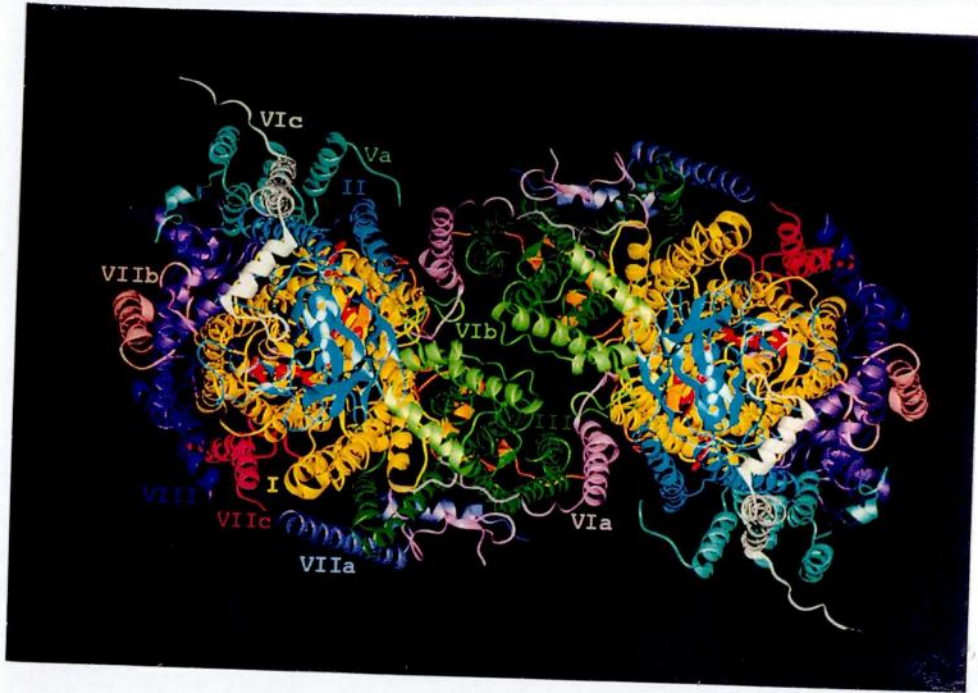
(b) A view from the cytosolic side.

Figure 3.2. The distribution of polar and non-polar amino acid residues.

Blue portions denote Cα atoms of polar amino acid residues, Arg, Asn, Asp, Gln, Glu, His, Lys, and Tyr while the Cα atoms of the other amino acid residues are yellow. Red sticks and balls denote hemes, Cu, Zn, and Mg atoms.
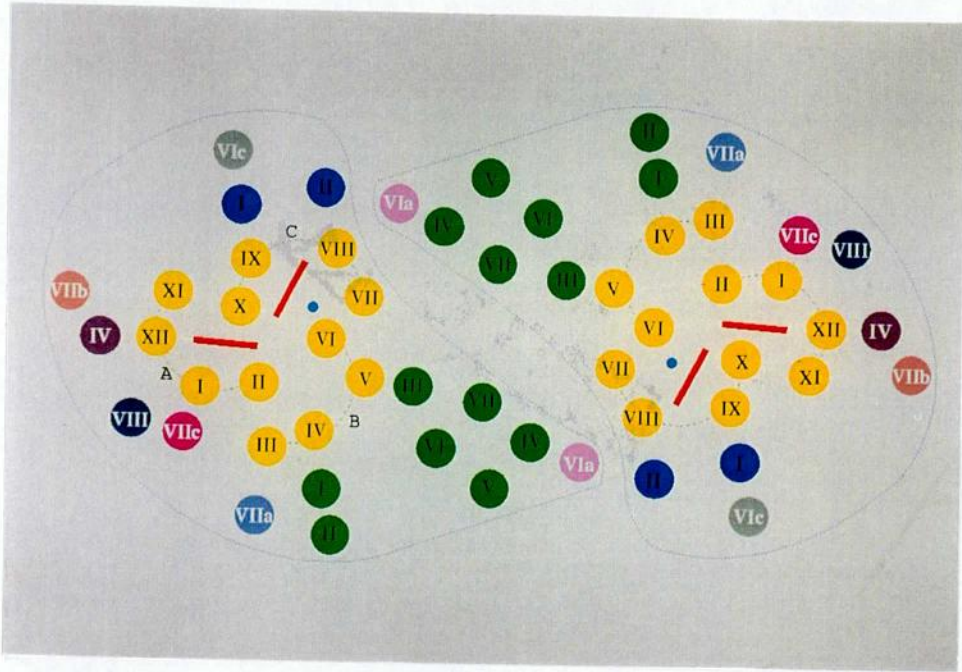
Figure 3.3. A schematic representation for location of transmembrane helices as a cross-section at the membrane surface of the cytosolic side.
Red bars and a small light blue ball denote heme planes and CuB, respectively. Black Roman numerals in yellow, blue, and green circles denote the helix number of subunits, **I**, **II**, and **III**, respectively. White letters in the other circles indicate nuclear coded subunits. The molecular surface of each monomer is shown by the dotted line. Broken lines denote semicircles observed in the helix arrangement of subunit **I**. The transmembrane helices form three semicircular arrangements, each composed of four helices: A(helices XI, XII, I, and II), B(helices III to VI), and C(helices VII to X).

dimensional structure on the transmembrane α helices with those predicted for subunits **I**, **II** and **III** from the amino acid sequences (Capaldi, 1990; Muller *et al.*, 1988; Raitio *et al.*, 1987) (Figure 3.4) indicates that the number of transmembrane α helices was correctly predicted. However, most of the real helical regions are longer than predicted ones, and an interhelix region between Val287 and Met297 in subunit **I**, which includes two Cu_B ligands, His290 and His291, was predicted to be part of a transmembrane α helix region. The presence of a transmembrane α helix has been successfully predicted for the nuclear-coded subunits from the analysis of the location of the NH_2-terminals and COOH-terminals, that is, seven of ten subunits have transmembrane regions (Capaldi, 1990) as shown in Figure 3.4.

## 3.2. Subunits encoded by mitochondrial genes

3.2.1. Subunit I

Subunit **I** is buried almost fully in the membrane and consists of 12 transmembrane helices that lack any large extramembrane parts (Figures 3.5a and 3.6). This subunit is cylindrical and is oriented perpendicular to

I
                                      I   50
MFINRWLFSTNHKDIGTLYLLFGAWAGMVGTALSLLIRAELGQPGTLLGD
                  II   100
DQIYNVVVTAHAFVMIFFMVMPIMIGGFGNWLVPLMIGAPDMAFPRMNNM
        III   150
SFWLLPPSFLLLLASSMVEAGAGTGWTVYPPLAGNLAHAGASVDLTIFSL
        IV   V 200
HLAGVSSILGAINFITTIINMKPPAMSQYQTPLFVWSVMITAVLLLLSLP
                                               VI   250
VLAAGITMLLTDRNLNTTFFDPAGGGDPILYQHLFWFFGHPEVYILILPG
                                    VII   300
FGMISHIVTYYSGKKEPFGYMGMVWAMMSIGFLGFIVWAHHMFTVGMDVD
            VIII   IX 350
TRAYFTSATMIIAIPTGVKVFSWLATLHGGNIKWSPAMMWALGFIFLFTV
                                          X   400
GGLTGIVLANSSLDIVLHDTYYVVAHFHYVLSMGAVFAIMGGFVHWFPLF
                         XI   450
SGYTLNDTWAKIHFAIMFVGVNMTFFPQHFLGLSGMPRRYSDYPDAYTMW
        XII   500
NTISSMGSFISLTAVMLMVFIIWEAFASKREVLTVDLTTTNLEWLNGCPP
        514
PYHTFEEPTYVNLK

II
                                            I   50
MAYPMQLGFQDATSPIMEELLHFHDHTLMIVFLISSLVLYIISLMLTTKL
                         II   100
THTSTMDAQEVETIWTILPAIILILIALPSLRILYMMDEINNPSLTVKTM
                                                     150
GHQWYWSYEYTDYEDLSFDSYMIPTSELKPGELRLLEVDNRVVLPMEMTI
                                                     200
RMLVSSEDVLHSWAVPSLGLKTDAIPGRLNQTTLMSSRPGLYYGQCSEIC
                                   227
GSNHSFMPIVLELVPLKYFEKWSASML

III
                                          I   50
MTHQTHAYHMVNPSPWPLTGALSALLMTSGLTMWFHFNSMTLLMIGLTTN
    II   III   100
MLTMYQWWRDVIRESTFQGHHTPAVQKGLRYGMILFIISEVLFFTGFFWA
                                             IV   150
FYHSSLAPTPELGGCWPPTGIHPLNPLEVPLLNTSVLLASGVSITWAHHS
    V   200
LMEGDRKHMLQALFITITLGVYFTLLQASEYYEAPFTISDGVYGSTFFVA
                                         VI   VII   250
TGFHGLHVIIGSTFLIVCFFRQLKFHFTSNHHFGFEAGAWYWHFVDVVWL
        261
FLYVSIYWWGS

IV   50

AHGSVVK SEDYA LPSYVDRRDYPLPDVAHVKNLS ASQKALKEKE KASWSS

                                                     I   100

LS IDEKVELYRLK FKES FAEM NRSTN EWKTVVGAAMFFIGFTALLLIWEK

                                                   147

HYV YGPIPHTF EEEWVAKQTKRMLD MKVAPIQGFSAKWDYDKNEWKK

VIa   I   50

ASAAKGDHGGTG ARTWRFLTFGLALPSVALCTLNSWL HSGHRERPAFIPY

                                     84

HHLRIRTKPFSWGDGNHTFFHNPRVNPLPTGYEK

VIc   I   50

STALAKPQMRG LLARRLRFHIVGAFMVSLGFATFYKFAVAEKRKKAYADF

                             73

YR NYD SMKDFEEMRK AGIFQSAK

VIIa   I   50

FENR VAEKQKLFQ EDNGLP VHLK GG ATDNILYRVTMTLCLGGTLYSLYCL

      56

GHASKK

VIIb   I   50

IHQKRAPD FHDKYGNAVLASGATFCVAVWVYMATQ IGIEWNPSPVGRVTP

      56

KEWREQ

VIIc   I   47

SHYEEGPGKNIPFSVEN KWRLLAMMTLFFGSGFAAPFFIVRHQLL KK

VIII   I   46

ITAKPAKTPTS PKEQAIGLSVTFLSFLLPAGWVLY HLDNYKKSSAA

Figure 3.4. Helix regions of subunits containing transmembrane moieties.

Rectangles show α-helical regions as determined from the crystal structure; underscoring highlights the α-helical regions predicted from the amino acid sequences. Bold and plain Roman numerals indicate the subunit name and number of each transmembrane helix.

Rectangles without a Roman numeral are α helices found in extramembrane region. No prediction for the transmembrane helix region of the nuclear coded subunits has yet been reported. Abbreviations for the amino acid residues are: A, Ala; C, Cys; D, Asp; E, Glu; F, Phe; G, Gly; H, His; I, Ile; K, Lys; L, leu; M, Met; N, Asn; P, Pro; Q, Gln; R, Arg; S, Ser; T, Thr; V, Val; W, Trp and Y, Tyr.
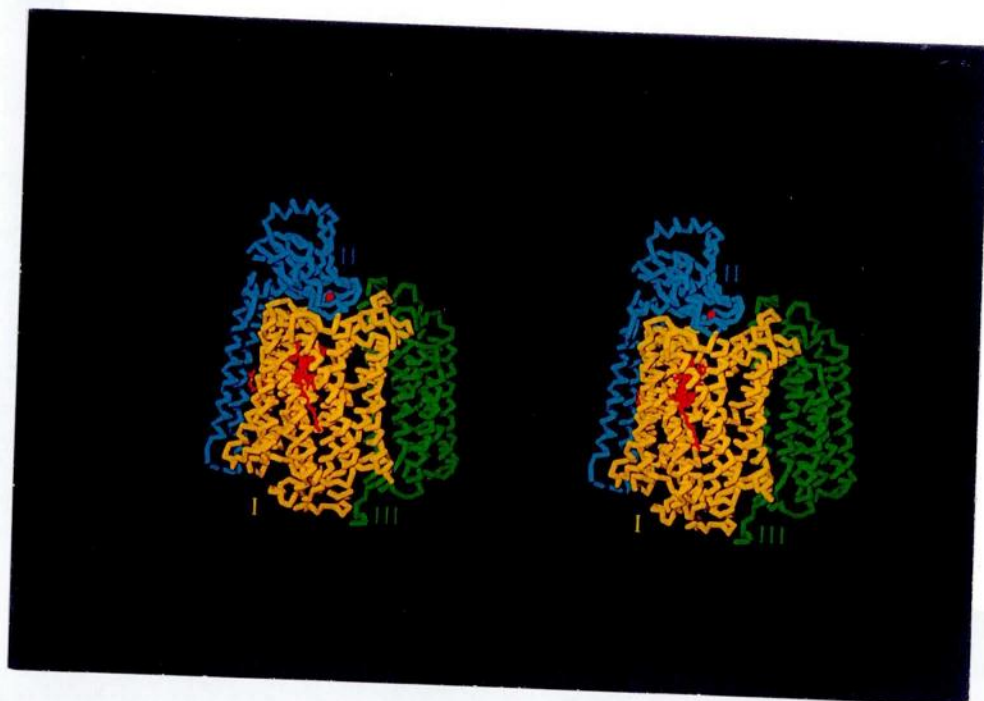
(a) Assembly of mitochondrial coded subunits.
Subunits **I** (yellow), **II** (blue), **III** (green).

Figure 3.5. Stereoscopic drawings of Ca-backbone trace for the 13 different subunits in separate figures.
Red models and balls in subunits **I** and **II** denote hemes and Cu atoms in CuA, respectively.
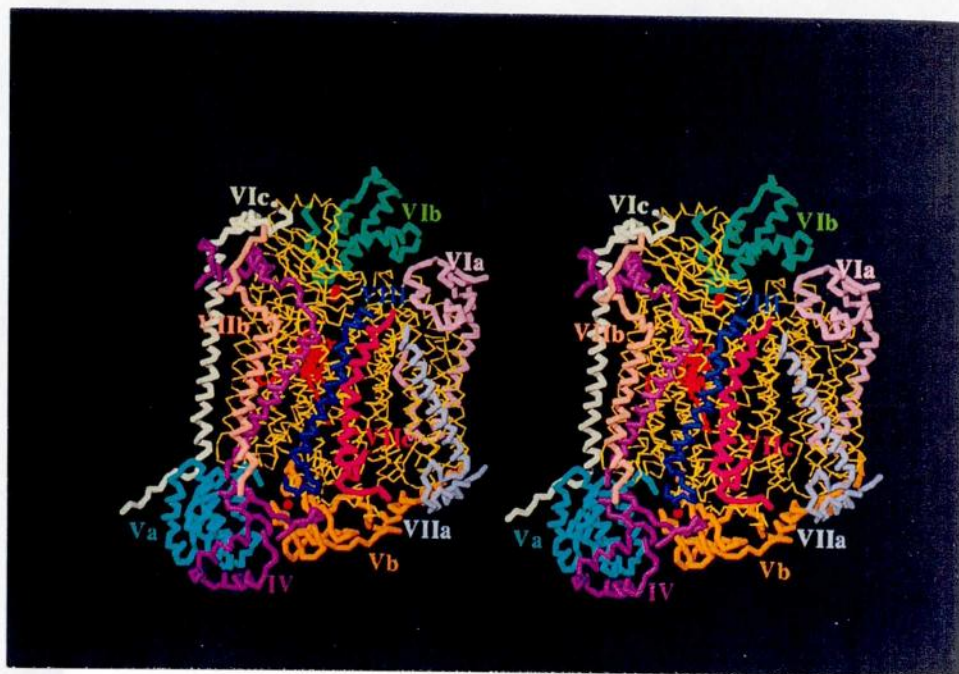
(b) Arrangement of nuclear coded subunits.
Subunits **IV**(purple), **Va** (sky blue), **Vb** (dark yellow), **VIa** (pale reddish violet), **VIb** (blue green), VIc (gray), **VIIa** (lavender), **VIIb** (beige), **VII** (pink), and **VIII** (indigo). A red ball in subunit **Vb** denotes the zinc atom. Subunits **I**, **II**, and **III** are shown by yellow thin stick models.

36
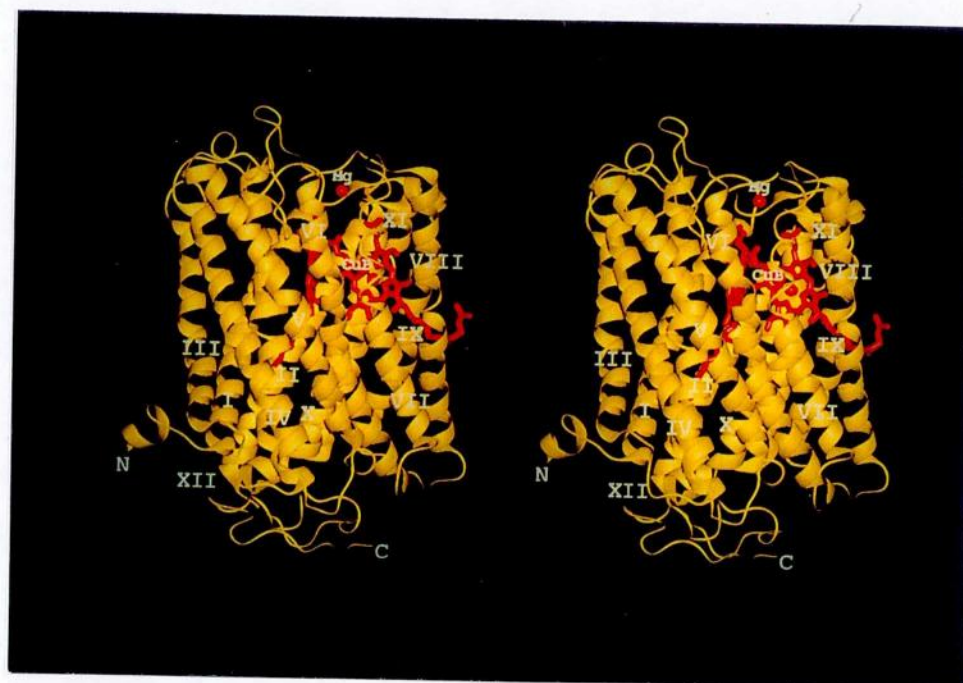
Figure 3.6. Structure of subunit I encoded by mitochondrial DNA (stereoscopic drawing).
Hemes a and a3, CuB and Mg are shown in red. Roman numerals denote the helix number of subunit I.

the membrane surface. The transmembrane helices form three semicircular arrangements, A, B, and C, each composed of four helices, helices XI, XII, I, and II, helices III to VI, and helices VII to X, respectively. The three semicircular arrangements form a "whirlpool" with a pseudo three-fold axis of symmetry (Figure 3.3). The arrangement of helices is fully consistent with the structure of the bacterial cytochrome *c* oxidase from *Paracoccus denitrificans* (Iwata *et al.*, 1995). The helices of subunit **I** are not completely perpendicular to the membrane surface plane. When the cytosolic surface of subunit **I** is "up", one end of each helix is placed on the top left and the other end on the bottom right so that they form angles of 20° to 35° with the normal of the membrane plane (Figure 3.6). Helices VI and VII are accessible to the intermonomer space of the dimeric enzyme, and helix XI is partly exposes to the lipid space of the membrane (Figure 3.3). The extramembrane portion in the NH_2-terminal region contains a two-turn α-helix, as shown in Figure 3.6. The starting and the ending points of the 12 helices are essentially at the membrane surface so that they make flat top and flat bottom surfaces to subunit **I** cylinder. The NH_2- and COOH-termini of subunit **I** are at

the matrix side, as shown in Figure 3.6. An extramembrane helix between the transmembrane helices IX and X is on the membrane surface of the cytosolic side, is also found in the bacterial enzyme (Iwata *et al.*, 1995). However, a nonhelical loop between helices III and IV (Figure 3.6) is reported to be α-helical in conformation in the bacterial enzyme (Iwata *et al.*, 1995).

Subunit **I** contains the prosthetic groups: hemes a and a$_3$, and Cu$_B$. The hemes are surrounded by two of the three semicircles, A (heme a) and C (heme a$_3$) (Figure 3.3), and are perpendicular to the membrane plane. The structure of the heme a and heme a$_3$-Cu$_B$ sites are shown in Figures 3.7 and 3.8. The iron atom of heme a has two histidine ligands: His378 in helix X at the 5th coordination site and His61 in helix II at the 6th coordination site. Both of His378 and His61 have hydrogen bonds with Val374 and Gly30, respectively (Figures 3.7). The hydroxyfarnesylethyl group of heme a is almost in an extended conformation and packs against helices I, II, X, and XII. The hydroxyl group of the hydroxyfarnesylethyl has a hydrogen bond with Ser382. The propionic acid groups of heme a interact through salt bridges and hydrogen bonds with Arg439, Arg438,
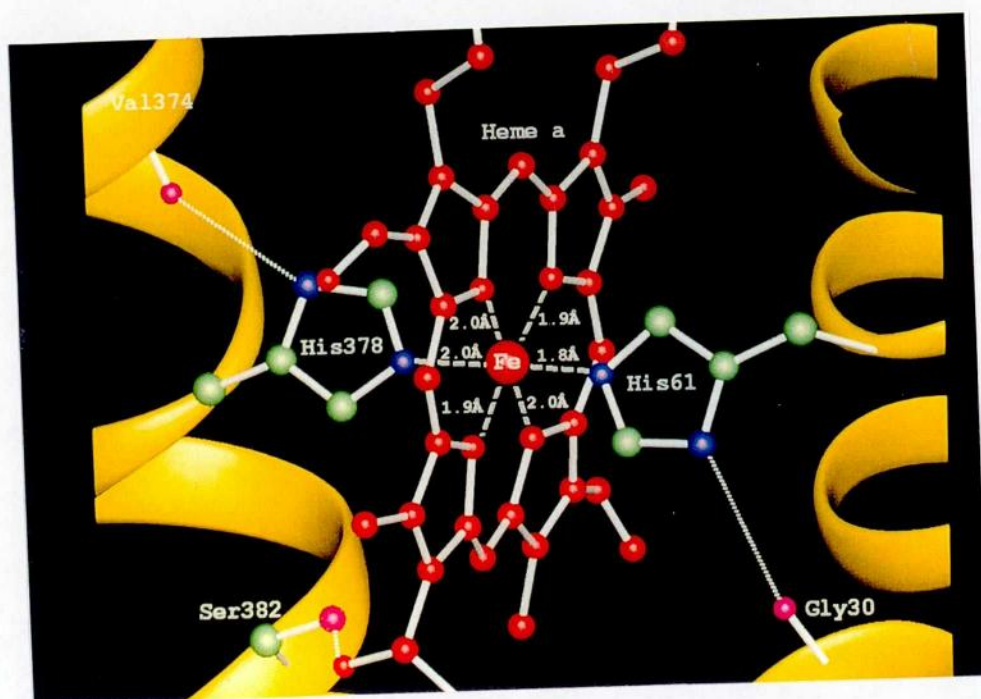
Figure 3.7. Coordination geometry of heme a site.
Green, indigo blue, and pink ball in ribbon model donate carbon, nitrogen, and oxygen atoms, respectively.
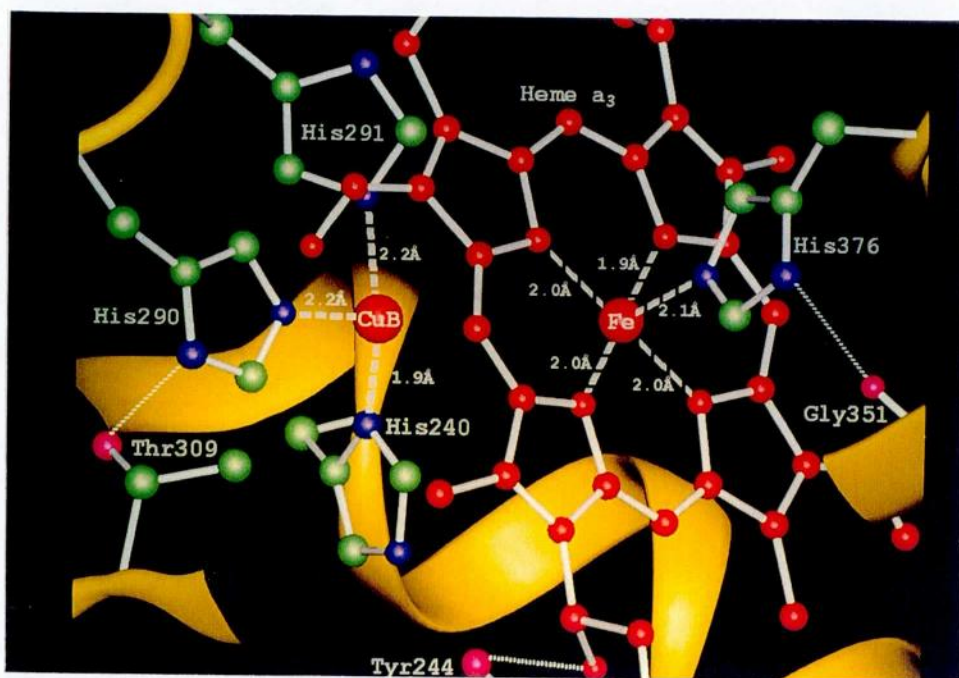
Figure 3.8. Coordination geometry of heme a₃-CuB site.
Green, indigo blue, and pink ball in ribbon model
donate carbon, nitrogen, and oxygen atoms,
respectively. The distance between Fe and Cu is 4.6 Å.

Tyr371, Trp126, and Tyr54. The pyrrole ring with a hydroxyfarnesylethyl side chain has close contact with Ser34. The pyrrole with a vinyl side group contacts closely with Met65. The pyrrole with methyl and propionic acid groups interacts with Phe377. Phe377 contacts closely with pyrrole ring of heme a_3 as that of heme a.

The fifth ligand of iron atom of heme a_3 is His376 in the helix X (Figure 3.8). This histidine residue makes a hydrogen bond with Gly351. The propionic acid groups of heme a3 interact through salt bridges and hydrogen-bonds with Arg438, Trp126, and His368. The twisted hydroxyfarnesylethyl group of heme a3 intersects the semicircle C (Figure 3.3) between helices VIII and IX. So far, the absolute configuration of the chiral carbon atom of the hydroxyfarnesylethyl group had not been known. The hydroxyfarnesylethyl group with S configuration carbon atom superimposes well with the MIR-DM electron density map (Figure 3.9). Thus, the absolute configuration was determined by the present X-ray analysis. The two hemes are bridged by the polypeptide segment of His376-Phe377-His378.

Cu_B is coordinated by three histidine residues (Figure 3.8), His240 in helix VI, His290 and His291 in
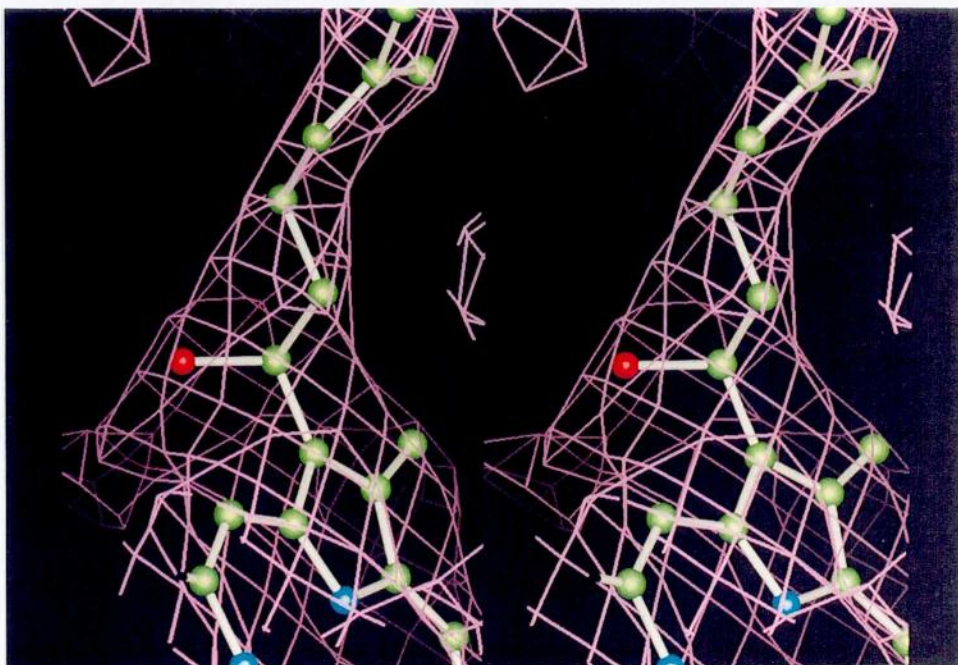
Figure 3.9. Fitting of the atomic model of hydroxyfarnesylethyl group with *S* configuration carbon atom to the electron density map (Stereoscopic drawing).

a nonhelical fragment between helices VII and VIII. His290 has a hydrogen bond with Thr309 (Figure 3.8). His291 has strong π-π stacking interaction with Trp236, as shown by stereoscopic drawing (Figure 3.10).

The complementary concaved surface of the cytosolic side of subunit **I** interacts strongly with the globular domain of subunit **II** (Figure 3.5a). The helix-helix interactions between helices VIII and XI of subunit **I** and helices II and I of subunit **II** in transmembrane part also stabilize the complex of subunits **I** and **II** (Figure 3.5a and Table 3.1). In addition to these interactions, subunit **I** also interacts with subunits **III**, **IV**, **V**, **VIIc**, and **VIII** as well as with subunit **II** by close helix-helix interaction in the membrane region (Figures 3.3 and 3.5, and Table 3.1). The COOH-terminus of subunit **I** is an extended segment that forms a β barrel structure of subunit **Vb**. Subunit **I** has no direct interaction with the extramembrane subunits **Va** and **VIb**, and the transmembrane subunit **VIc**. Subunit **VIa** is a transmembrane subunit that has no close contact with subunit **I** in the transmembrane part, but a part of its extramembrane domain interacts with subunit **I**.
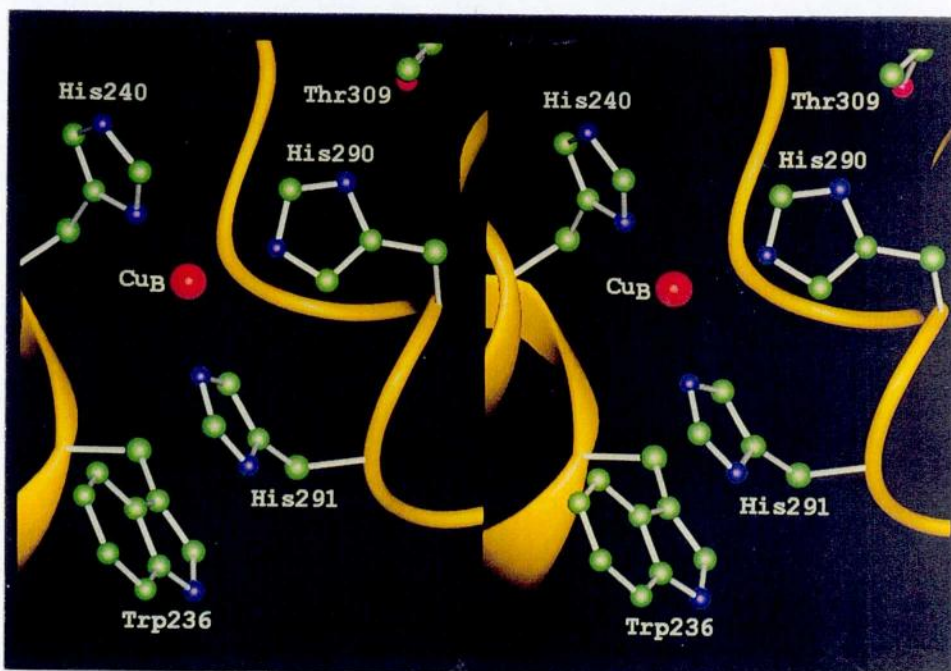
Figure 3.10. The structure around Cu$_B$ as viewed from heme a$_3$ (stereoscopic drawing).

Table 3.1. Geometries of interaction between two adjacent transmembrane α helices.

Inclination degree	Orientation	Adjacent helices*
~0	antiparallel	II(**I**)-III(**I**), VI(**I**)-VII(**I**), X(**I**)-XI(**I**), IX(**I**)-I(**II**)
~20	parallel	I(**I**)-III(**I**), II(**I**)-IV(**I**), III(**I**)-I(**III**), I(**III**)-I(**VIIa**), I(**IV**)-I(**VIIb**), I(**VIIc**)-I(**VIII**)
~20	antiparallel	I(**I**)-II(**I**), I(**I**)-XII(**I**), III(**I**)-IV(**I**), IV(**I**)-V(**I**), V(**I**)-VI(**I**), VII(**I**)-VIII(**I**), VIII(**I**)-IX(**I**), IX(**I**)-X(**I**), XI(**I**)-XII(**I**), VIII(**I**)-II(**II**), IV(**I**)-I(**III**), I(**II**)-I(**VIc**), I(**III**)-II(**III**), II(**III**)-I(**VIIa**), III(**III**)-IV(**III**), III(**III**)-VII(**III**), IV(**III**)-V(**III**), V(**III**)-VII(**III**), V(**III**)-VI(**III**), VI(**III**)-VII(**III**), IV(**III**)-I(**VIa**), I(**IV**)-I(**VIII**)
~50	parallel	II(**I**)-VI(**I**), II(**I**)-X(**I**), VI(**I**)-X(**I**), I(**I**)-I(**VIIc**), I(**I**)-I(**VIII**), V(**I**)-III(**III**), XI(**I**)-I(**V**)
~50	antiparallel	II(**I**)-V(**I**), IV(**I**)-III(**III**), XII(**I**)-I(**IV**), XII(**I**)-I(**VIII**)

*Each helix is denoted by a helix number followed by **a subunit number** in parenthesis.

3.2.2. Subunit II

Subunit **II** is composed of three parts, an NH_2-terminal extended structure, two transmembrane helices and a globular extramembrane domain (Figures 3.5a and 3.11). The globular domain above the cytosolic surface of subunit **I** consists of the COOH-terminal 139 residues and forms a 10-strand β barrel structure as well as a three-turn α-helix that consists of the last 10 COOH-terminal residues. The NH_2-terminal 14 residues exhibit an extended structure within the intermembrane space. Both the NH_2- and COOH-termini of subunit **II** are located on the cytosolic side, as shown in Figure 3.11.

The dinuclear copper center of Cu_A is held by the loops of the β barrel, as shown in Figure 3.11. The Cu_A site consists of six ligands, two cysteines (Cys196 and Cys200), two histidines (His161 and His204) a methionine (Met207), and a peptide carbonyl of a glutamate (Glu198), as shown in Figure 3.12. Except for His161 which is in β strand 6, the other ligands are all in an extended structure between β strands 9 and 10. His161 forms a hydrogen bond with Asp158 that is exposed on the molecular surface. His204 has a hydrogen bond with a peptide bond between Arg438 and Arg439 of subunit **I**. The two copper atoms are bridged by two
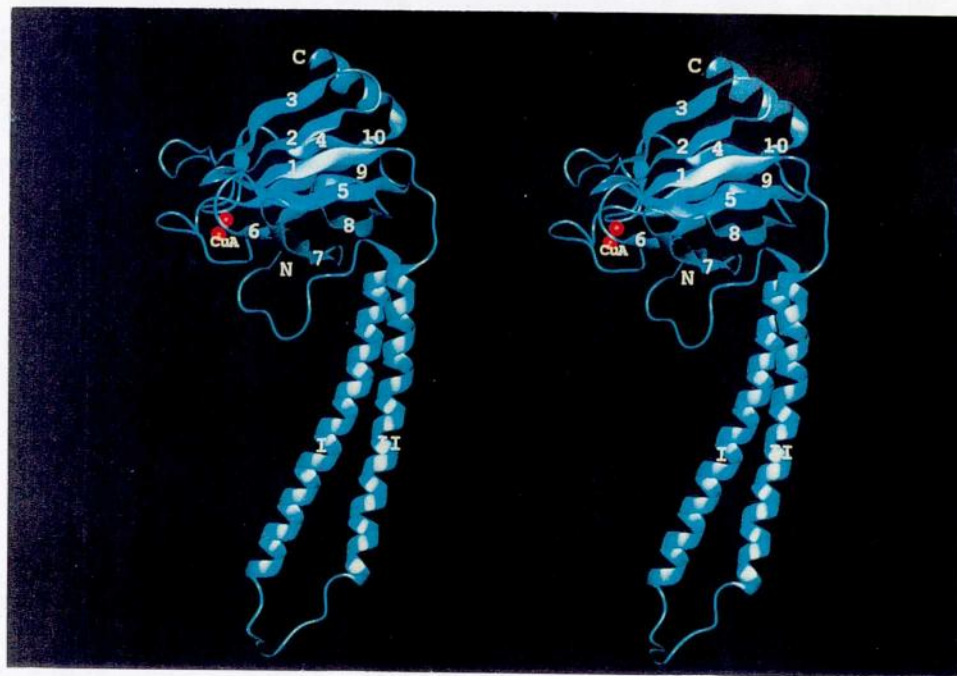
Figure 3.11. Structure of subunit II encoded by mitochondrial DNA (stereoscopic drawing).
Figure contains CuA site(red). Roman numerals and Arabic numerals denote the helix number and the β strand number of subunit **II**, respectively.
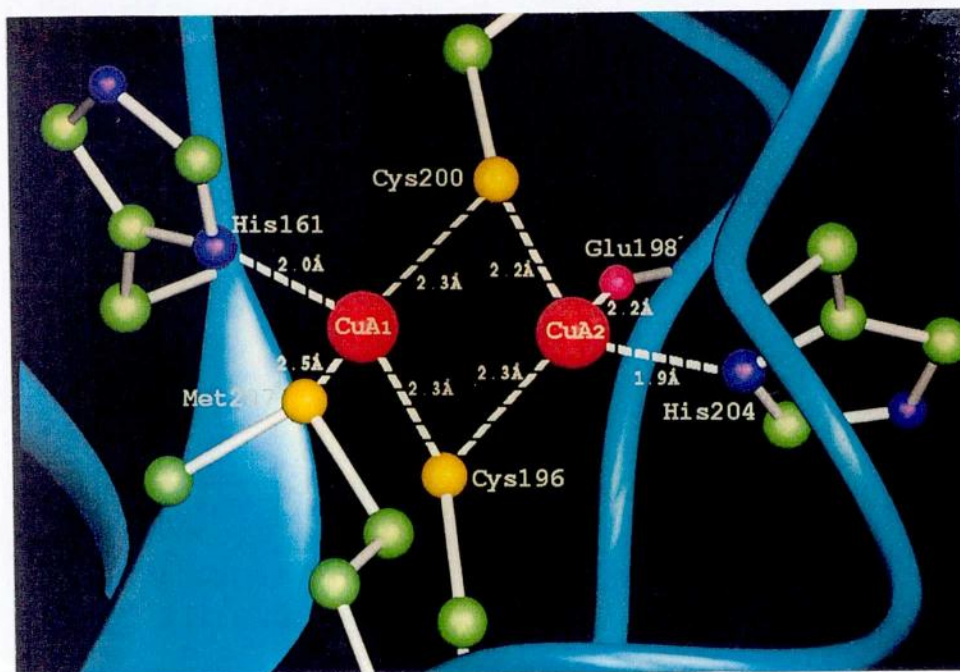
Figure 3.12. Coordination geometry of Cu$_A$ site.

The interatomic distances of Cu-Cu and Sγ-Sγ are 2.3 Å and 3.9 Å, respectively. Angles of CuA site are shown the following:

Cys196-Cu1-Cys200, 117.38°; Cys200-Cu2-Cys196, 121.54°
Cys196-Cu1-Met207, 113.87°; Cys200-Cu2-Glu198, 113.72°
Cys196-Cu1-His161, 125.94°; Cys200-Cu2-His204, 123.36°
Cys200-Cu1-Met207, 98.34°; Cys196-Cu2-Glu198, 89.12°
Cys200-Cu1-His161, 101.69°; Cys196-Cu2-His204, 112.34°
Met207-Cu1-His161, 94.08°; Glu198-Cu2-His204, 84.73°
Cu1-Cys196-Cu2, 60.29°; Cu1-Cys200-Cu2, 60.65°

sulfur atoms of Cys196 and Cys200. Each copper atom forms a tetrahedral coordination including the two cysteine sulfur atoms (Figure 3.12). The geometry is similar to that of a [2Fe-2S]-type iron-sulfur center (Tsukihara *et al.*, 1981), in which the Fe ions and inorganic sulfur atoms are replaced with Cu ions and cysteine sulfur atoms.

Both the two transmembrane helices and the extramembrane domain interact strongly with subunit **I**, as described previously. Helix I interacts with subunit **VIc** on the opposite side against the molecular surface contacting with subunit **I** in the transmembrane region (Figure 3.3 and Table 3.1). The extramembrane domain has close contacts with subunits **IV**, **VIb** and **VIc** on the cytosolic side, as shown in Figure 3.5b.

3.2.3. Subunit III

Subunit **III** contains seven transmembrane helices and no extensive extramembrane domain (Figures 3.5a and 3.13). The NH_2-terminus is on the matrix side. A big V-shaped cleft is formed by two NH_2-terminal helices, I and II, in an antiparallel arrangement and a bundle of five other helices. Four helices of the bundle, IV, V, VI, and VII form a typical four-helix bundle structure
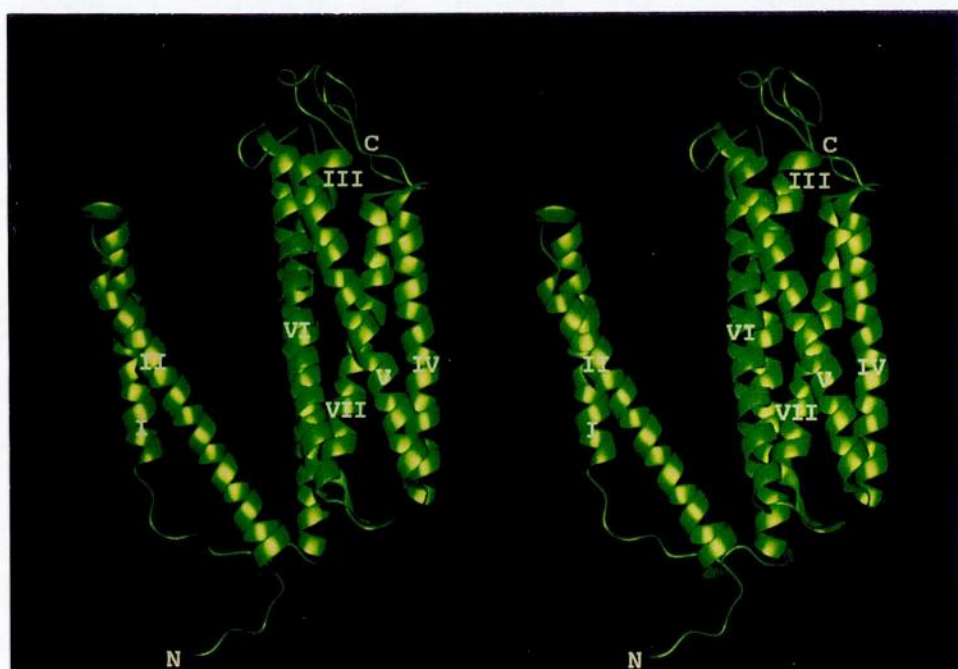
Figure 3.13. Structure of subunit III encoded by mitochondrial DNA.
Stereo view of subunit III viewed approximately parallel to the membrane. Roman numerals denote the helix number of subunit III.

such that any closest pair of helices is antiparallel (Figure 3.13).

The interface between subunits **I** and **III** is made by helices III and IV of subunit **I** packing against helix I of subunit **III**, and helices IV and V of subunit **I** packing against helix III of subunit **III**, (Figure 3.5a). The helices are not all parallel to each other. Helix I of subunit **III** is at an angle of 20° to helices III and IV of subunit **I**. Similarly, helix III of subunit **III** is at an angle of 50° to helices IV and V of subunit **I** (Table 3.1). The extramembrane domain of subunit **VIa** overlays the V-shaped cleft of subunit **III**, as shown in Figure 3.5b. The bottom side of the cleft is much narrower than the top side and is sealed with an extramembrane α helix from the NH_2-terminal region of subunit **VIIa** (Figure 3.5b). However, the other side of the transmembrane surface is exposed to the external medium (Figure 3.3).

3.3. Nuclear coded subunits

Nuclear coded subunits associate with the surface of the three core subunits encoded by mitochondrial genes, but leave many areas uncovered, especially on the cytosolic side. All the NH_2-terminal ends of

transmembrane helices of the nuclear coded subunits are placed on the matrix side and the COOH-terminal ends on the cytosolic side (Figure 3.14). The locations are consistent with those predicted by crosslinking analysis (Capaldi, 1990), except for subunits **VIII** and **VIa**, whose NH$_2$-termini were assigned to be located on the cytosolic side (Zhang *et al.*, 1988; 1991).

Subunits having a transmembrane helix

3.3.1. Subunit IV

Subunit **IV** looks like a dumbbell with the transmembrane helix in the middle and the two extramembrane domains on either end, as shown in Figure 3.14. The cytosolic domain is composed of the 41 COOH-terminal residues in an extended structure that contains a four-turn α-helix and interacts with subunits **II** and **VIIb**. The NH$_2$-terminal matrix domain folds into a globular structure with two one-turn α-helices and two three-turn α-helices. It interacts strongly with subunit **Va**. The transmembrane helix contacts diagonally helices XI and XII of subunit **I** (Figures 3.3 and 3.5b) at an angle of 50°. The transmembrane helix of subunit **IV** associates with
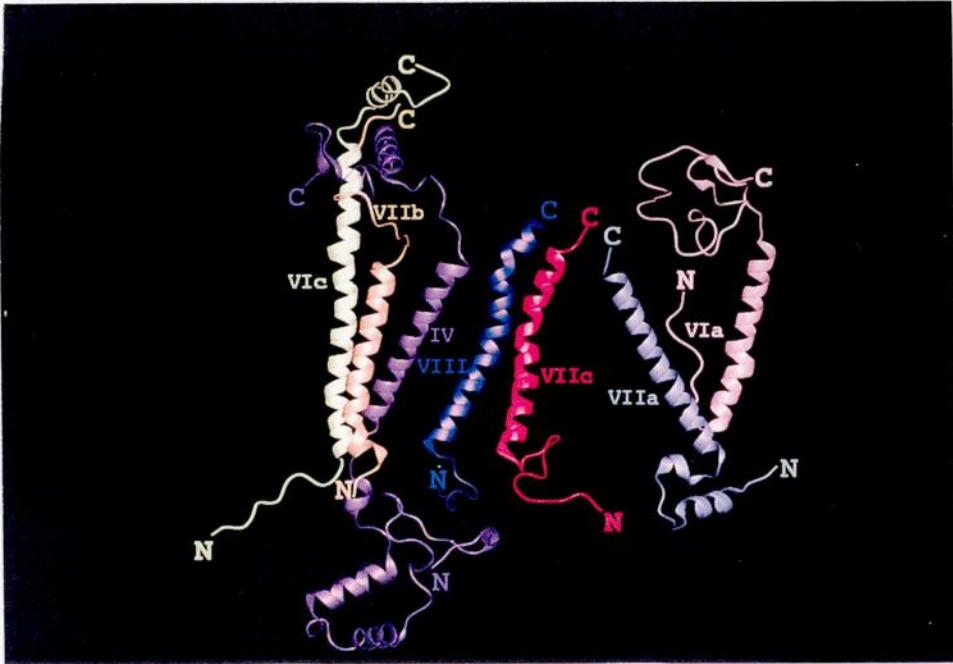
Figure 3.14. Structure of nuclear coded subunits with a transmembrane helix.
Each of the seven nuclear coded subunits has a transmembrane helix. All the COOH-terminal ends are placed on the cytosolic side.

subunits **VIIb** and **VIII** as well as subunit **I** (Figure 3.14 and Table 3.1). The transmembrane helix of subunit **IV** is sandwiched between helix XII of subunit **I** and the subunit **VIIb** helix.

3.3.2. Subunit VIa

The COOH-terminal 40 residues form a globular structure on the cytosolic side that interacts with the subunits **I** and **III**, and covers the cleft of subunit **III** at the cytosolic side. The transmembrane helix interacts with helix IV of subunit **III** on the opposite side of the attachment point of subunit **III** to subunit **I** and makes contact with the other monomer (Figures 3.3 and 3.5b). The NH_2-terminal ten residues are in an extended conformation in the transmembrane region and contact with helices V and VII of subunit **I** of the other monomer (Figure 3.3). These contacts seem likely to stabilize the dimeric structure. The electron density distribution for the ten NH_2-terminal residues is less clear than that for the other part of the protein moiety.

3.3.3. Subunit VIc

Subunit **VIc** is also a dumbbell type subunit with a long transmembrane helix contacting to helix I of subunit **II**, an extended peptide segment composed of the NH$_2$-terminal 11 residues on the matrix side, and the COOH-terminal 21 residues which fold into a three-turn α-helix parallel to the membrane surface on the cytosolic side (Figures 3.5b and 3.12). This subunit interacts with subunit **II** at both the membrane region and the cytosolic side and with subunit **Va** at the matrix side as shown in Figures 3.5a and b.

3.3.4. Subunit VIIa

Subunit **VIIa** has a transmembrane helix with the NH$_2$-terminal domain consisting of two helices with one turn and three turns on the matrix side, but has no residues on the cytosolic side (Figure 3.14). The three-turn α helix at the NH$_2$-terminus is in plane of the membrane surface on the matrix side. The helix makes a rectangular turn at the membrane surface and covers the cleft of subunit **III** at the bottom together with the subunit **Vb** (Figure 3.5b). The transmembrane helix stands against subunit **III** with the COOH-terminus on the cytosolic side near the COOH-terminus of subunit

56

VIIc. It interacts with helix I of subunit **I** and helices I and II of subunit **III** at the membrane region (Figures 3.3 and 3.5b and Table 3.1).

3.3.5. Subunit VIIb

Subunit **VIIb** has a transmembrane helix with an extended structure of the COOH-terminal 21 residues at the cytosolic side, and with only a few residues at the matrix side. This subunit contacts closely with subunit **IV** at both of the transmembrane and the intermembrane spaces (Figures 3.3 and 3.5b).

3.3.6. Subunit VIIc

Subunit **VIIc** has a transmembrane helix which is kinked at middle and has a NH_2-terminal small extramembrane moiety in a irregular conformation at the matrix side (Figure 3.14). The COOH-terminus is at the membrane surface of the cytosolic side and interacts with helices I, II, and III of subunit **I** and the COOH-termini of subunits **VIIa** and **VIII**. This subunit is adjacent to subunit **VIII** on the surface of subunit **I** and is placed so that it packs closely at a diagonal to helices I and XII of subunit **I**.

3.3.7. Subunit VIII

Subunit **VIII** with a short NH_2-terminal extended structure on the matrix side is adjacent to and parallel with the transmembrane helix of subunit **IV**. It makes close diagonal contacts with helix I of subunit **I** in the upper transmembrane region (Figure 3.3) and helix XII of subunit **I** in the lower transmembrane region (Figure 3.5b).

Extramembrane subunits

3.3.8. Subunit Va

Subunit **Va** is on the matrix side below subunit **I** and contains five α helices. Each α helix has four to five turns that are oriented so that together the five α helices form a right-handed superhelix (Andy-Mark et al., 1994). This is also a one-turn α-helix in an extended structure in the COOH-terminal region, as shown in Figures 3.5b and 3.15. This subunit is held without any direct contact with subunit **I** by the matrix domain of subunit **IV** and the extramembrane segment of subunit **VIc** (Figure 3.5b). The shortest distance between atoms of subunits **I** and **Va** is 6.5 Å, indicating

Figure 3.15.   Structure of subunit Va (stereoscopic drawing).

Subunit **Va** consists of five α helices.

that bulk water may freely enter into the space between the two subunits.

3.3.9. Subunit Vb

Subunit **Vb** is below subunits **I** and **III**, adjacent to subunit **Va** and toward the extramembrane domain of subunit **IV**, but without direct contact with subunits **IV** and **Va** (Figure 3.5b). The subunit attaches tightly to the bottom surfaces of subunits **I** and **III**. The COOH-terminal domain of this subunit forms a β-barrel structure (Figure 3.16), involving an extended segment of subunit **I**, in which a tetrahedral zinc site with four cysteine ligands is located (Figure 3.17). The NH_2-terminal region is in an extended conformation interacting with subunit **III**. A three-turn α-helix segment links the two domains (Figure 3.16). The subunit folds in an abnormally extended conformation, which is stable only in the subunit assembly.

This subunit has a zinc site (Tsukihara et al., 1995) with four cysteines and a zinc finger motif (Härd et al., 1990) in the amino acid sequence between Cys60 and Cys85. However, the conformation determined by crystal structure does not suggest any physiological role as a zinc finger. Three cysteines ligating to the
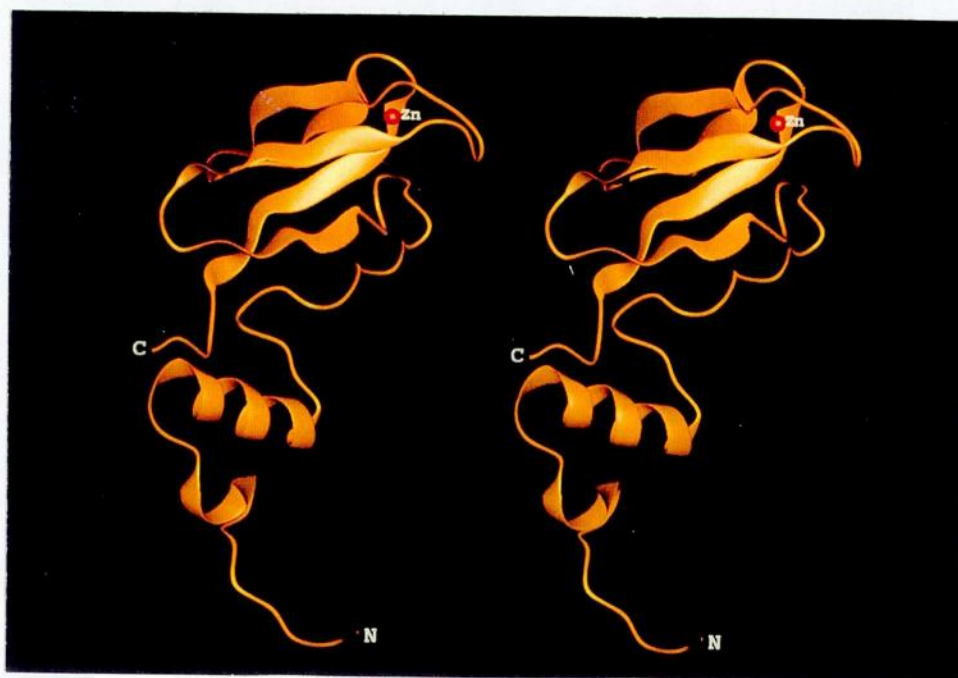
Figure 3.16. Structure of subunit Vb (stereoscopic drawing).

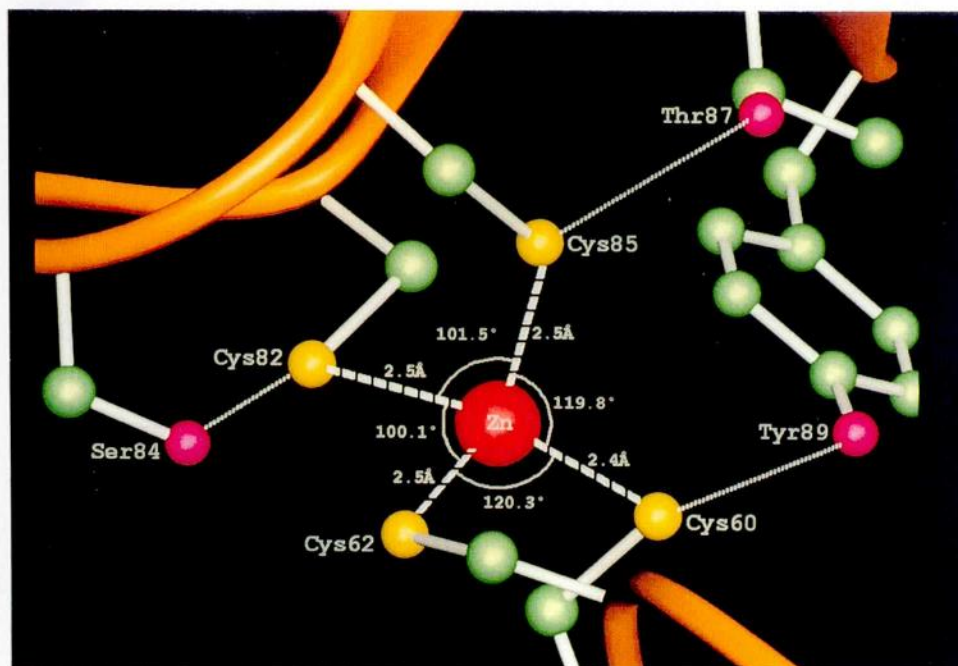Zn (red ball) is held in the β barrel with eight β strands.

Figure 3.17. Geometry of zinc site.

zinc atom, Cys60, Cys82, and Cys85, have hydrogen bonds with Tyr89, Ser84, and Thr87, respectively (Figure 3.17).

3.3.10. Subunit VIb

Subunit **VIb** is the only subunit without transmembrane helix at the cytosolic side. This subunit associates with subunits **II** and **III** (Figure 3.5b). Two disulfide bridges are present between Cys29 and Cys64 and between Cys39 and Cys53, as shown in Figure 3.18. The segment between Cys 39 and Cys53 is involved in an intermonomer contact with the corresponding segment on the other monomer around the two-fold symmetry axis (Figure 3.1a). This structure as well as the NH_2-terminal ten residues of subunit **VIa** is in contact with the other monomer as described earlier. This intermolecular interaction between the two subunits related by a pseudo two-fold symmetry seems to stabilize the dimeric state.
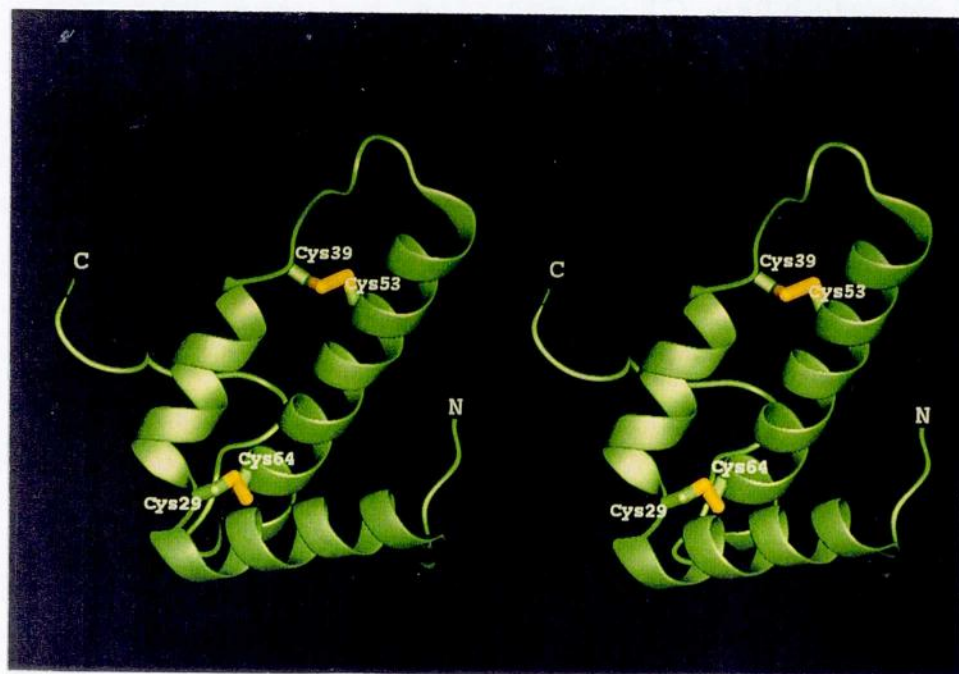
Figure 3.18. Structures of Subunit VIb (stereoscopic drawing).
The disulfide bridges are shown in yellow.

3.4. Discussion of the structure

The most specific structural feature of this membrane protein complex is the 56 transmembrane α helices. All of the transmembrane part of the photosynthetic reaction center (Deisenhofer, 1984), also consists of α helices. The other membrane proteins determined at high resolution, the Porins, have a β barrel structure in the transmembrane region. All the other transmembrane structures determined at low resolution exhibit α helices. Thus we can conclude that membrane proteins tend to fold into secondary structures such as α helices and β sheets. α helices seem to be favored for membrane proteins with long hydrophobic regions such as cytochrome *c* oxidase. Why does a protein fold into α helix? When a protein is in aqueous solution, the final location of the side chains inside the protein makes a large contribution to the free energy of stabilization due to the hydrophobic effect (Kauzmann, 1959). However in membrane proteins, other effects should dominate the free energy of stabilization. The presence of nonaqueous solvents often stabilizes the formation of hydrogen-bonded, regular secondary structures, because of the lack of competing hydrogen bonds by water molecules.

Consequently, α helixes are strongly favored over other irregular configurations in the membrane (Haltia *et al.*, 1995). The hydrophobic effect also makes a significant contribution to the membrane partitioning and stability of a transmembrane helix. Therefore, it is reasonable that most transmembrane parts of membrane proteins with long hydrophobic regions consist of α helices.

Another specific feature of the bovine heart cytochrome *c* oxidase is an abundant distribution of irregular structure at the level of the membrane surface. This enzyme contains not only hydrophobic but also hydrophilic residues in these regions. Interactions of both of the main chains and the hydrophilic side chains with phosphate groups of the membrane can contribute to stability of the molecular structure. As these hydrophilic interactions are prominent in this region, irregular main chain structures which are unfavorable for the main chain conformation in other environments may be often found.

Most of the transmembrane helices are not vertical to membrane plane and usually are not parallel to each other. Each pair of the nearest neighbor helices in our crystal structure fits one of three types of stable

helix-helix interactions, namely, crossing at one of three angles, approximately, 0°, 20°, or 50° (Table 3.1) (Chothia, 1977). These interactions contribute to the stability of the enzyme molecule and to inter-subunit recognition.

The three subunits encoded by mitochondrial genes that form the core of this enzyme resemble those of the bacterial enzyme in main chain fold and subunit arrangement. The other subunits encoded by nuclear genes surround the core subunits. This structural arrangement suggests that these three subunits assemble just after they are synthesized in the mitochondria, and nuclear encoded subunits are associated with the surface of core subunits. The process of molecular evolution from the bacterial enzyme to the mammalian enzyme effects this hierarchy of structural organization.

All the NH_2-terminal ends of nuclear encoded subunits with a transmembrane helix are located on the matrix side. This structural feature suggests that these subunits find their own sites on the surface of core subunits without penetrating the mitochondrial inner membrane after insertion into the mitochondrial

inner membrane from the cytosolic side led by the NH_2-terminals.

Subunits **VIa** and **VIb** are in contact with the other monomer. The overall shape of the monomer and the extent of the intermonomer interaction suggest that the mitochondrial enzyme may function in dimeric state under physiological conditions. Since these two subunits which contribute to the intermonomer interaction are nuclear encoded proteins, the dimeric state may not be attained in the bacterial enzyme, which lacks these subunits. In the eukaryotic enzyme, there may be additional functions for the dimeric enzyme. Research on this topic has just been initiated by several persons.

The histidine ligands to hemes a and a_3 all make hydrogen bonds with main chain carbonyls in helices. These hydrogen bonds may stabilize the coordination geometry of the hemes. The coordination of hemes a and a_3 are both affected by their electronic state. Thus the histidine residues coordinating to the hemes a and a_3 can mediate structural changes from the hemes to the transmembrane helices on reduction and oxidation of the iron atoms. These structural changes may act to couple

the proton pumping functions with oxygen reduction at the active center.

Each of the iron atoms is in their heme plane. As heme a with ferric iron exhibits tetragonal bipyramidal coordination, the location of iron in the heme plane is quite reasonable. However the tetragonal pyramidal coordination of the heme a_3 iron is not consistent with the iron being ferric. The recent difference Fourier synthesis with coefficients of $(Fo-Fc)\exp(i\alpha c)$ clearly showed significant difference density between Fe_{a3} and Cu_B. The difference density may correspond to an oxygen atom or dioxygen atoms. Existence of an atom ligating to Fe_{a3} is more consistent with the planar structure of the Fe_{a3} coordination.

Chapter 4.

Possible channels observed in three dimensional structure

4.1. Structures participating in proton transfer

Protons are transferred most effectively through hydrogen bonds, particularly in a hydrophobic environment such as the transmembrane region of this enzyme. Thus, we searched for any structure that could participate in a hydrogen-bond network. Neither the network spanning across the transmembrane region from the matrix side to the cytosolic side nor the one from the matrix side to the Fea_3-Cu_B site which is the oxygen reduction site was detectable in current crystal model. Nevertheless, many cavities (spaces with no detectable electron density distribution) inside the molecule connect short hydrogen-bond systems or pairs of functional groups that could participate in hydrogen-bonded relay system. These cavities are likely to contain water molecules and thus to conduct protons readily. Furthermore, there are many points where there is space for a conformational change of side chain that would induce a new hydrogen-bond system (possible hydrogen-bond structure). The following three networks

in subunit **I** are candidates for the proton channels in the enzyme (Figures 4.1a, b, and c).

First network.

The main part of a network that involves residues in helices III and IV of subunit **I**, as shown in Figure 4.1a. At the entrance of this network are His503 and Asn11, both in extended loops and connected with a fixed water through hydrogen bonds. The fixed water is at the terminal of a hydrogen-bond linkage involving three water molecules connected with Asp91 and Asn98. The fixed water at the other end of the hydrogen-bond linkage is at a position to form hydrogen bond with either Ser101 or Tyr19 with a small conformational change. Tyr19 is connected by two hydrogen bonds and a fixed water to Ser156. The three OH groups of Tyr19, Ser101, and Ser156 could form hydrogen bonds between them by a small conformational change. A cavity connects the Ser156 with Ser157, which is hydrogen-bonded to a fixed water. The water is connected by a cavity to Ser108, which is hydrogen-bonded to Ser149. Another cavity connects the two hydrogen-bond systems, Ser108-Ser149 and Thr146-Ser115. Finally, the network is connected to Ser142 via a possible hydrogen-bond structure.
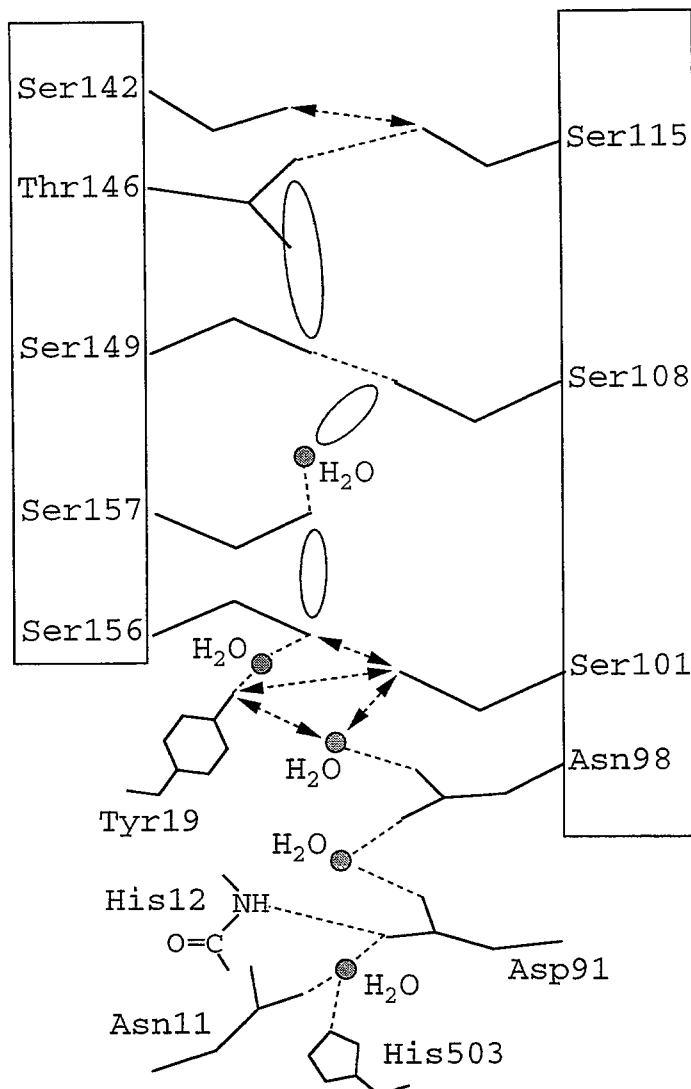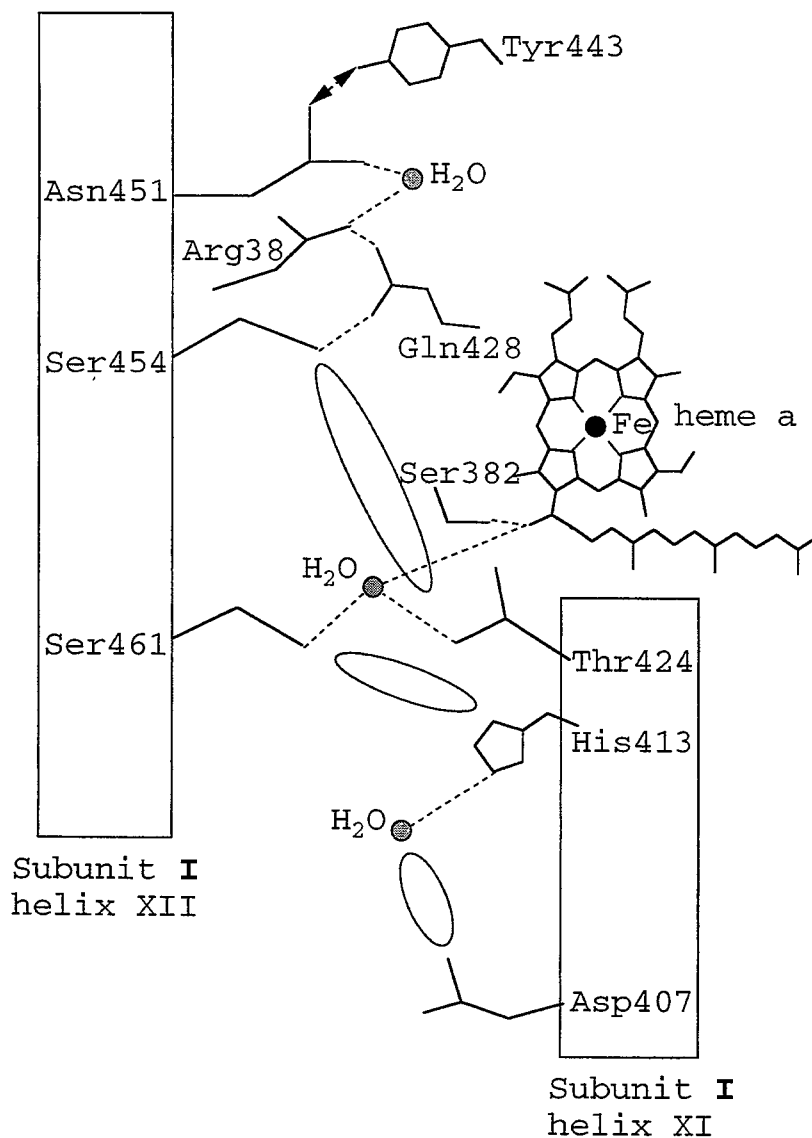
(a) The first network (a possible channel for proton pumping).
At the entrance of this network are His503 and Asn11, connected with a fixed water through hydrogen bonds. The channel terminates at hydrogen bond between Ser142 and Ser115. This channel contains four other possible hydrogen-bond structures between Tyr19, a fixed water hydrogen-bonded to Asn98, Ser101 and Ser156

Figure 4.1. Schematic representations of candidates for proton channel.
Dark ovals, dotted lines, and dotted lines with arrows denote internal cavities, hydrogen bonds, and possible hydrogen-bond structure, respectively. The size and shape of the cavities are not drawn quantitatively.

(b) The second network (a possible channel for proton pumping).
This network contains Asp407 at the entrance of the network on the matrix side and only one possible hydrogen bond structure between Asn451 and Tyr443. A branch leading to heme a could control the proton transfer along the main stream by redox changes in heme a.
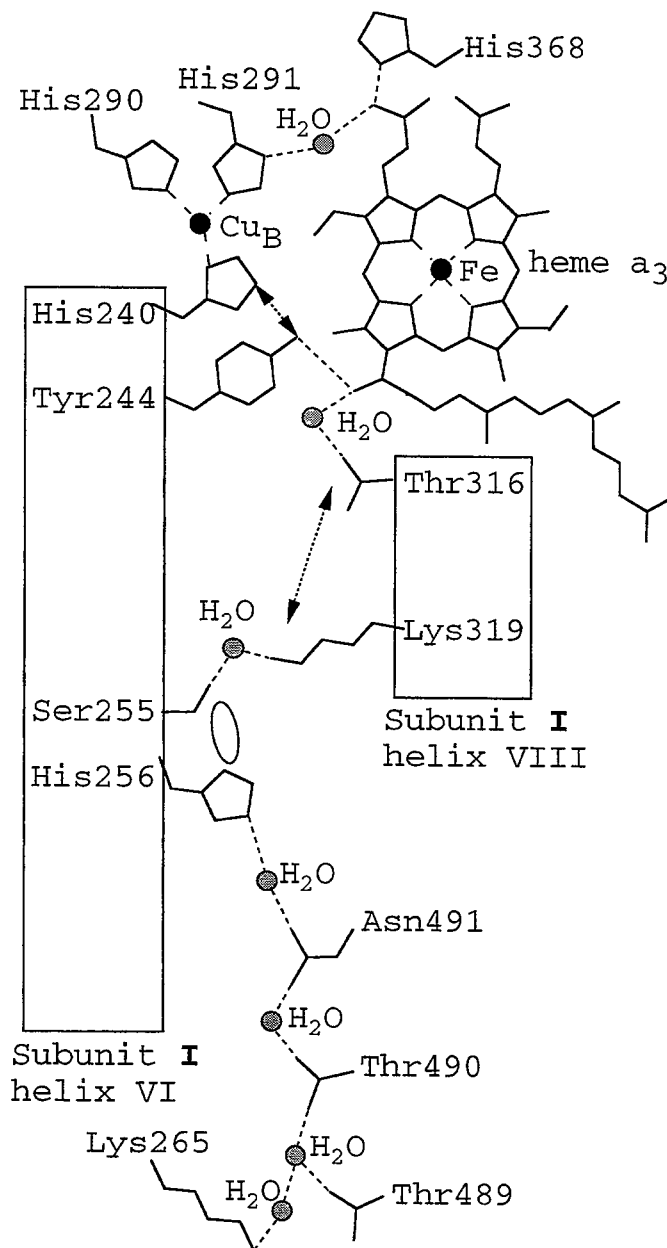
(c) The third network (a possible channel for protons for releasing water).
This network involving heme a3 spans from Lys265 at the matrix side to Tyr244 which is connected to His240, a ligand to CuB, by a possible hydrogen-bond structure. The other possible hydrogen-bond structure is between Lys319 and Thr316. Since this network ends at the ligand to CuB, it is most likely to work as a channel for protons to form water molecules.

All the amino acids in the network are well conserved, although in some species serine or threonine are replaced with alanine or glycine. Because of the small size of these residues, they could form cavities to contain water and still allow proton transfer.

Second network.

This network is located mainly between helices XI and XII of subunit **I**, as shown in Figure 4.1b. Asp407 at the entrance of the network at the matrix side and His413 are connected by a fixed water and a cavity. The imidazole of His413 is connected by another cavity to Ser461. A fixed water molecule forms a bridge between Ser461, Thr424 and the hydroxyl of the hydroxyfarnesylethyl side chain of heme a, via three hydrogen bonds. The hydrogen bond system is extended to Ser382 through the OH group of the farnesyl chain. The third hydrogen bond to heme a leads to a dead end at Ser382, providing a possible control of proton transfer along the main stream by redox change in heme a. The Thr424 is connected by a cavity to Ser454, which is a terminal of another hydrogen-bond system including Gln428, Arg38, a fixed water and Asn451. The Asn451 and Tyr443 are connected by a possible hydrogen-bond

structure. The last three residues, Arg38, Asn451, and Tyr443 are highly conserved during molecular evolution.

Third network.

This network involves helices VI and VIII of subunit **I** and heme a$_3$, as shown in Figure 4.1c. At the entrance, Lys265 is placed and connected to Thr490 via two fixed waters. One of the waters closer to Thr490 is hydrogen-bonded also to Thr489, perhaps stabilizing the arrangement of the two water molecules. The hydrogen-bond linkage is extended up to His256 via Asn491 and two water molecules. The His256 is connected with Lys319 via a cavity, Ser255 and a fixed water molecule hydrogen-bonded between Ser255 and Lys319. The Lys319 is connected by a possible hydrogen-bond structure to Thr316. A fixed water forms two hydrogen bonds to Thr316 and the OH of the hydroxyfarnesylethyl group of heme a$_3$, which is hydrogen-bonded to Tyr244. The Tyr244 is connected by a possible hydrogen-bond structure to His240, one of the ligands of Cu$_B$. Since this network ends at the ligand to Cu$_B$, it is most likely to work as a channel for protons to form water molecules. However it cannot be excluded that this system serves also as a proton pump via His240, Cu$_B$, and possibly His291, which

is the end of a hydrogen-bond system leading to a water channel as described below.

The above three networks form an equilateral triangle in subunit **I** when viewed from the cytosolic side such that the proton channel leading to the dioxygen reduction site is equidistant from the two possible proton pumping channels (Figure 4.2)..

A proton pumping pathway to the dioxygen reduction site by way of Ser157, Glu242, and His290 from an entrance on the matrix side including Asp91 has been proposed for the bacterial enzyme (Iwata *et al.*, 1995). The bottom part of the first network as given above seems essentially the same as that proposed, up to Ser157. Our crystal structure contains a cavity connecting Ser157 with Glu242, as in the case of the bacterial enzyme. However, His290 is located far from Glu242, giving no evidence of a possible proton transfer in our crystal structure.
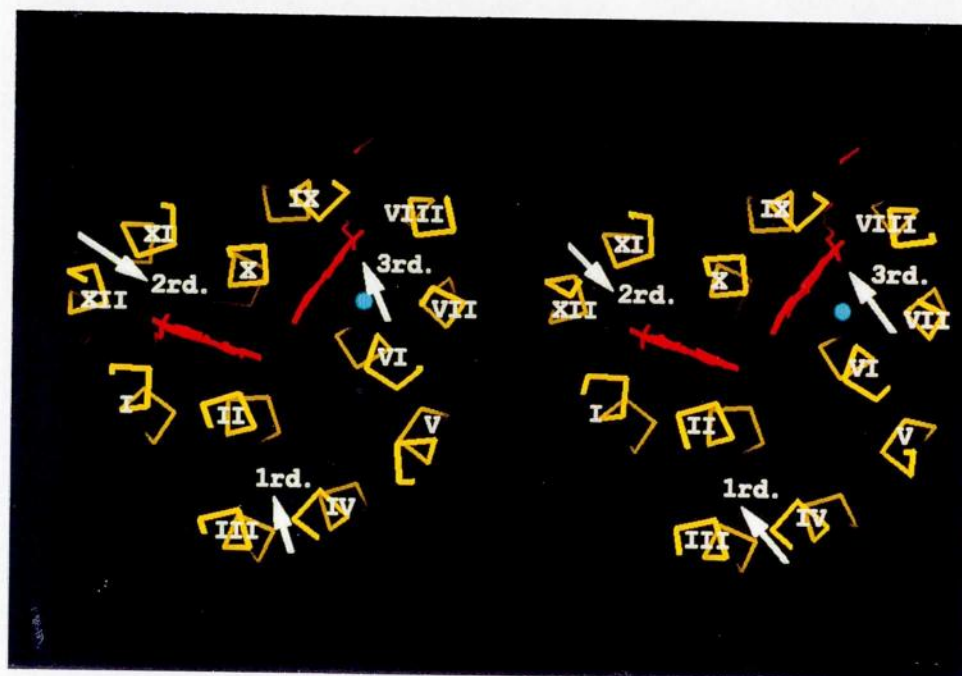
Figure 4.2. A schematic representation for location of three networks (stereoscopic drawing).
Red models and blue point denote hemes a and a3 and CuB, respectively. Roman numbers denote helix number of subunit **I**.

4.2. Possible water channel

A structure that could serve as a water channel for removing H_2O produced at the O_2 reduction site (Figure 4.3), proceeds from propionates at the cytosolic side of heme a3 along the subunits **I-II** interface to the cytosolic surface of the enzyme. The magnesium site and the propionates of heme a3 form a hydrophilic environment that includes two basic amino acids (Arg438 and His368 of subunit **I**), one acidic amino acid (Asp364 of subunit **I**), the two propionates of heme a3, and two fixed water molecules, all of them connected with one another by hydrogen bonds. The hydrophilic region is connected to a channel formed on the interface between subunits **I** and **II** with loose arrangement of hydrophilic residues that could provide a water channel to the cytosolic surface with small conformational changes. The amino acids of subunit **II** contributing to the channel are Glu198 ligating to the magnesium, Asp173, Asn180, and Arg178 arranged from the Mg site to the cytosolic surface of the enzyme. The amino acids of subunit **I** are placed in the channel; Thr294, Tyr129, Gln232, His233, and Asp227, directing to the cytosolic end. All the above amino acids placed in the possible channel are well conserved in most
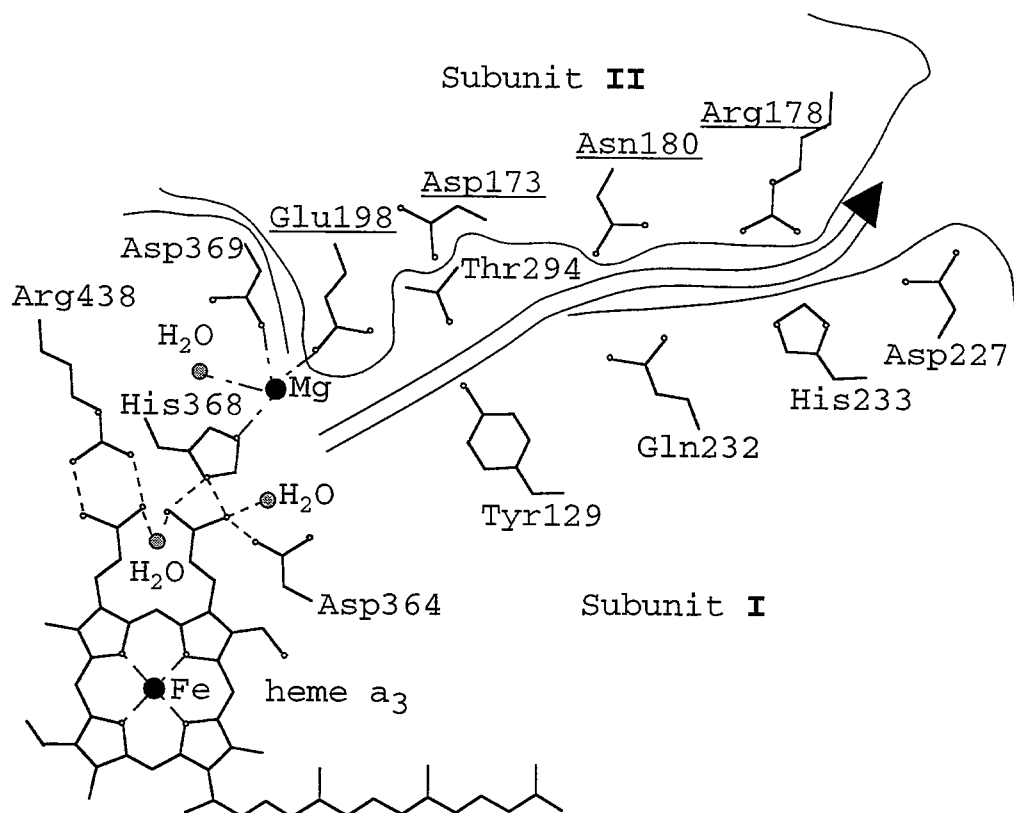
79

Figure 4.3. Schematic representations of candidates for water channel.
The underlined residue names and numbers denote the residues of subunit **II**. Small circles in the amino acid model are polar atoms. The arrow denote a possible water channel from the O_2 reduction site to the open end at the cytosolic side.

species reported so far, implying a common mechanism for removing water from the Fea_3-Cu_B site. The possible channel in the crystal structure does not have enough space for water molecule to pass through freely, which seems indispensable for preventing proton leak from the cytosolic side.

4.3. Possible dioxygen channels

No space through which a dioxygen molecule (O_2, a rod-shaped molecule with diameter of 2.4 Å) can reach the oxygen reduction site from the molecular surface is detectable, as in the case of hemoglobin and myoglobin (Perutz, 1990). In analogy to these globins, the conformation with an open channel for O_2 seems attained only during one of the many reversible and rapid conformational changes so that the population of the conformation is too low to detect by X-ray crystallography (Caughey et al., 1981; Potter et al., 1990). However, the O_2 channel (or channels) is probably located in the following three areas near the Fea_3-Cu_B site, where most of amino acid side chains in the area are hydrophobic and packed loosely.

O$_2$ first channel.

Cu$_B$ occurs very near the molecular surface faced
to inter-monomer space of the dimeric structure where
no other subunit is placed. On the molecular surface
nearest to Cu$_B$, Phe237 of subunit **I** is located, as
shown in Figure 4.4a. Next to the Phe237, Trp288,
Trp236, and His291 are located on line up to Cu$_B$. These
side chains, as well as other side chains nearby,
provide a hydrophobic environment from the molecular
surface to the Cu$_B$ site, as shown in Figure 4.4a. These
residues, which are well conserved, indicate the
importance of the hydrophobicity.

O$_2$ second channel.

Dioxygen molecules could approach to the dioxygen
reduction site from the V-shaped cleft (the lipid pool)
in subunit **III** which is likely to keep the hydrophobic
dioxygen molecules (Figure 4.4a). Starting from His151
on the surface of subunit **I** exposed to the lipid pool
of subunit **III**, a network of hydrophobic amino acids
including Leu199, Phe67, Phe238, Phe235, Trp126, and
Trp236, approaches to the Fea$_3$-Cu$_B$ site.

O$_2$ third channel.

The third candidate for the dioxygen channel
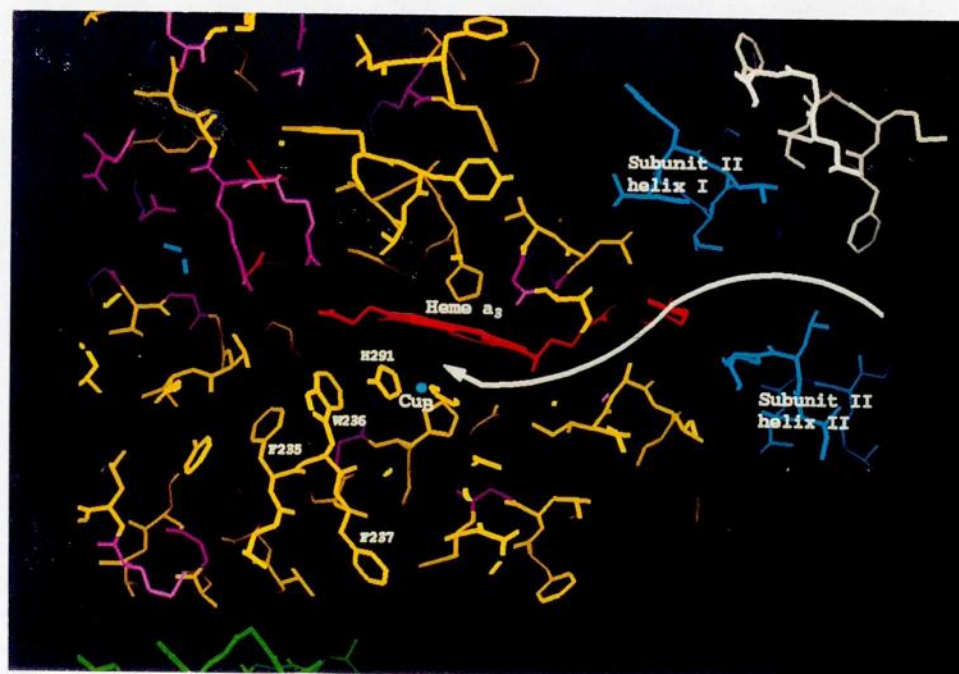includes the hydroxyfarnesylethyl group of heme a$_3$. The
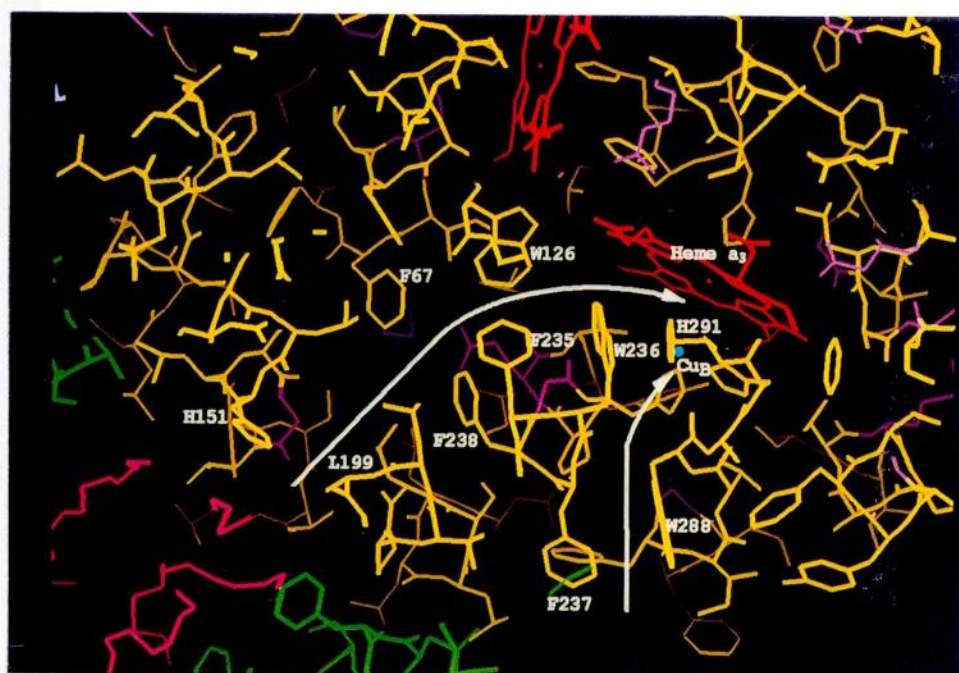
(a) Possible channels reaching CuB.
A pink structure is phospholipid in the lipid pool of
subunit III.

Figure 4.4. Possible O2 channels.
Red structures are hemes. Blue, green, and white amino
acid residues belong to subunits II, III, and VIc,
respectively. Yellow amino acid residues are aromatic
or hydrophobic in subunit I. The white arrows indicate
the possible pathways of O_2.

(b) Channel by way of hydroxyfarnesylethyl group.

terminus of the hydroxyfarnesylethyl group is placed very close to the surface of subunit **I** (Figure 4.4b). The nearest point on the surface of subunit **I** to terminal of the long alkyl group is accessible to the membrane space between the two attaching points of the two transmembrane α helices of subunit **II**. The environment of the alkyl group is hydrophobic with loosely packed amino acid side chains so that the dioxygen could pass through to the oxygen binding site with a little change in the conformation around the alkyl group.

All the above three channels may be effective under physiological conditions in order for attaining the extremely high affinity of the enzyme to O_2.

Chapter 5.

Conclusion

The MIR method with ordinary heavy atoms was successfully applied to the phase determination of a large molecule with 408,000 molecular weight. Solvent flattening as well as non-crystallographic symmetry averaging was very powerful for the phase refinement for the membrane protein complex.

This is the first membrane protein complex from a higher organism determined at atomic resolution and the most complicated structure known at atomic resolution. This enzyme has a dimeric structure in the crystal and may be a dimer in it's native state. All the transmembrane part of the dimeric enzyme consists of 58 α helices. Irregular structures are abundant in the membrane protein at the phosphate level.

The mitochondrial subunits form a core particle resembling the *Paracoccus denitrificans* enzyme, while the nuclear subunits surround the core subunits. This is the first hybrid protein, which consists of proteins from two different organelles. Subunit **Va** has a novel super-secondary structure of right-handed helical α helices. The absolute configuration of

hydroxyfarnesylethyl group is determined as *S* with the MIR-DM electron density map.

Three candidates for proton channels were identified in the three dimensional structure of the enzyme. Oxygen channels were also assigned in the structure. A water channel was clearly found in the border between subunits **I** and **II**.

These results could not be expected and will effect the future progress of various research on cytochrome *c* oxidase and membrane protein complexes.

References

Anderson, S., de Bruijin, M. H. L., Coulson, A. R.,
Eperon, I. C., Sanger, F. & Young, I. G. (1982).
J. Mol. Biol. **156**, 683-717.

Andy-Mark, H. W. et al. (1994). *Nature* **367**, 750

Aoyama, H. (1996).

Babcock, G. T. & Wikström, M. (1992). *Nature* **356**, 301-
309.

Biewald, R. & Buse, G. (1982). *Hoppe-Seyler's Z.
Physiol. Chem.* **363**, 1141-1153.

Blow, D. M., & Crick, F. G. C. (1959). *Acta
Crystallogr.* **13**, 794-802.

Brooks, B., Bruccoleri, R., Olafson, B., States, D.,
Swaminathan, S., & Karplus, M. (1983). *J. Comp.
Chem.* **4**, 187-217.

Brünger, A. T. (1988). *J. Mol. Biol.* **203**, 803-816.

Brünger, A. T. (1992). *Nature* **355**, 472-475.

Buse, G., & Steffens, G. J. (1978). *Hoppe-Seyler's Z.
Physiol. Chem.* **359**, 1005-1009.

Capaldi, R. A. (1990). *Annu. Rev. Biochem.* **59**, 569-596.

Caughey, W. S., Shimada, H., Choc, M. G., & Tucker, M.
P. (1981). *Proc. Natl. Acad. Sci. U.S.A.* **78**, 2903-
2907

Cawtan, K. (1994). in *Joint CCP4 and ESF-EACBM Newsleter on Protein Crystallography* **31**, 34-38.

Chothia, C., Levitt, M., & Richardson, D. (1977). *Proc. Natl. Acad. Sci. U.S.A.* **74**, 4130-4134

Deisenhofer, J., Epp, O., Miki, K., Huber, R. & Michel, H. (1984). *J. Mol. Biol.* **180**, 385-398.

Einersdottir, Ó., Dyer, R. B., Lemon, D. D., Killough, P. M., Hubig, S. M., Atherton, S. J., López-Garriga, J. J., Palmer, G. & Woodruff, W. H. (1993). *Biochemistry* **32**, 12013-12024.

Einersdottir, Ó. & Caughey, W. S. (1985). *Biochem. Biophys. Res. Commun.* **129**, 840-847.

Engh, R. A. & Huber, R. (1991). *Acta Cryst.* **A47**, 392-400.

Erdewd, M. Buse, G. (1985). *Hoppe-Seyler's Z. Physiol. Chem.* **366**, 257-263.

Fuller, S. D., Capaldi, R. A. & Henderson, R. (1979). *J. Mol. Biol.* **131**, 305-327.

Haltia T. & Freire, E. (1995). *Biochem. Biophys. Acta* **1241**, 295-322

Härd, T., Kellenbach, E., Boelens R., Maler B. A., Dahlman K., Freedman L. P., Carlstedt-Duke J., Yamamoto K. R., Gustatsson J. A., Kaptein J. A. (1990). *Science* **249**, 157-160

Iwata, S., Ostermeier, C., Ludwig, B., & Miche, H. (1995). *Nature* **376**, 660-669.

Kadenbach, B., Ungibaver, U., Jaraush, J., Buge, U. & Kuhn-Neutwig, L. (1983). *Trends Biochem. Sci.* **8**, 398-440.

Kauzmann, W. (1959). *Adv. Protein. Chem.* **14**, 1-63

Luzzati, V. (1952). *Acta Cryst.* **5**, 802-810.

Malatesta, F., Antonini, G., Sarti, P., & Brunori, M. (1995). *Biophysical Chemistry* **54**, 1-33

Malmström, B. G. (1990). *Chem. Rev.* **90**, 1247-1260.

Meineck, L., Steffens, G. J. & Buse, G. (1984). *Hoppe-Seyler's Z. Physiol. Chem.* **365**, 313-320.

Meineck, L. & Buse, G. (1985). *Hoppe-Seyler's Z. Physiol. Chem.* **366**, 687-694.

Meineck, L. & Buse, G. (1986). *Hoppe-Seyler's Z. Physiol. Chem.* **367**, 67-73.

Muller, M., Labonia, N. & Azzi, A. (1988). *Biochem. Biophys. Res. Commun.* **154**, 1260-1265

Otwinowski, Z. (1991). MLPHARE, *CCP4 Proc.*, 80, Daresbury Laboratory, Warrington, UK.

Perutz, M. F. *Mechanism of Cooperativity and Allosteric Regulation in Proteins* (Cambridge Univ. Press, Cambridge, 1990)

Potter, W. T., Hazzard, J. H., Choc, M. G., Tucker, M. P. & Caughey, W. S. (1990). *Biochemistry* **29**, 6283-6295

Raitio, M., Jalli, T. & Saraste, M. (1987). *EMBO J.* **6**, 2825-2833.

Ramakrishman, C. & Ramachandran, G. N. (1965). *Byophys. J.* **5**, 909-933.

Satcher, R., Steffens, G. J. & Buse, G. (1979). *Hoppe-Seyler's Z. Physiol. Chem.* **360**, 1385-1392.

Steffens, G. C., Steffens, G. J. & Buse, G. (1979). *Hoppe-Seyler's Z. Physiol. Chem.* **360**, 1641-1650.

Steffens, G. C. M., Biewald. R., T. & Buse, G. (1987). *Eur. J. Biochem.* **169,** 295-300.

Tanaka, M., Haniu, M. Yasunobu, K. T., Yu, C. A., Yu, L., Wei, Y. H. & King, T. E. (1979). *J. Biol. Chem.* **254**, 3879-3885.

Tsukihara, T., Fukuyama, K., Nakamura, M., Katsube, Y., Tanaka, N., Kakudo, M., Hase, T., & Matsubara, H. (1981). *J. Biochem.* **90**, 1763-1771.

Tsukihara, T., Aoyama, H., Yamashita, E., TomiZaki, T., Yamaguchi, H., Shinzawa-Itoh, K., Nakashima, R., Yaono, R., & Yoshikawa, S. (1995). *Science* **269**, 1069-1074.

Wang, B. C. (1985). *Methods Enzymol.* **115**, 90-112.

Warburg, O. & Negelein, E. (1929). *Biochem. Z.* **214**, 64–100.

Yanamura, W., Zhang, Y. Z., Takamiya, S., & Capaldi, R. A. (1988). *Biochemistry* **27**, 4909-4914.

Zhang, Y. Z., Lindorfer, M. A., & Capaldi, R. A. (1988). *Biochemistry* **27**, 1389-1394.

Zhang, Y. Z., Ewart, G., & Capaldi, R. A. (1991). *Biochemistry* **30**, 3674-3681.

List of Publications

1. The Whole Structure of the 13-subunit Oxidized Cytochrome *c* Oxidase at 2.8 Å

T. Tsukihara, H. Aoyama, E. Yamashita, T. Tomizaki, H. Yamaguchi, K. Shinzawa-Itoh, R. Nakashima, R. Yaono and S. Yoshikawa

(1996). *Science* **272**, 1136-1144.

2. Structures of Metal Sites of Oxidized Bovine Heart Cytochrome *c* Oxidase at 2.8 Å

T. Tsukihara, H. Aoyama, E. Yamashita, T. Tomizaki, H. Yamaguchi, K. Shinzawa-Itoh, R. Nakashima, R. Yaono and S. Yoshikawa

(1995). *Science* **269**, 1069-1074.

3. Effects of Ethyleneglycol Chain Length of Dodecyl Polyethyleneglycol Monoether on Crystallization of Bovine Heart Cytochrome *c* Oxidase.

K. Shinzawa-Itoh, H. Ueda, S. Yoshikawa, H. Aoyama, E. Yamashita and T. Tsukihara

(1995). *J. Mol. Biol.* **246**, 572-575.